Collecting Shells in the Tides: Formation of Dwarf Galaxies From Mergers Inside Galaxy Clusters

Anna Ivleva

Munich 2023

Kinder der Gezeiten:
Entstehung von Zwerggalaxien durch Kollisionen in Galaxienhaufen

Anna Ivleva

München 2023

Collecting Shells in the Tides: Formation of Dwarf Galaxies From Mergers Inside Galaxy Clusters

Anna Ivleva

Master's Thesis

at the University Observatory Munich

Ludwig Maximilian University

Submitted by

Anna Ivleva

born in Rostow

Supervised by

Dr. Rhea-Silvia Remus

Prof. Klaus Dolag

Lucas M. Valenzuela

Munich – November 22, 2023

Contents

Introduction

"Why would anyone pour milk over the sky?" Millennia ago, a thought like this – or maybe similar – crossed the minds of humans gazing up into the night. The desire to find reason and purpose for the things we see around us seems to be deeply rooted into our minds. The long established name for our home galaxy, the Milky Way, is not only reflecting this pursuit for explanation, but is also a showcase for our inherent associative thinking: in the attempt to describe and understand something, we first start by categorizing it in terms of what we already know. Such also the night sky, by finding patterns and giving names to recognizable constellations. There must have been a turning point sometime, when people started wondering what exactly they were seeing, and why it was there in the first place. Following the road of such deceptively simple questions has led to staggering discoveries and plot twists in the understanding of our place in the world – with the promise of much more yet to come.

1.1 Travelling Through Cosmic History

Our Universe is believed to have formed in an instantaneous event 13.8 Gyr ago, which is commonly referred to as the Big Bang (cf. Figure 1.1). It was followed by the inflationary epoch, a brief but extremely rapid expansion of the Universe. During this period, present quantum fluctuations got "stretched out" to such extent, that they left an imprint as approximately gaussian perturbations in the matter density field, which are ultimately accounted responsible for subsequent structure formation (Mukhanov, 2005). But the Universe was not quite there yet – it was so hot and dense that it took a few minutes too cool down enough by the continued expansion to build atomic nuclei in an episode called primordial nucleosynthesis. However, conditions were still too extreme to capture electrons and form neutral atoms. The plasma was therefore tightly coupled to radiation, because photons interacted with free electrons via Thomson scattering. As soon as the temperature dropped below the threshold for stable atoms, the mean free path for photons increased, allowing them to move independently. This moment of recombination defines a surface of last scatter, beyond which it is impossible to see. The released photons can be observed nowadays in the microwave band – hence referred to as cosmic microwave background (CMB) – and constitute the oldest observable light in our Universe. Decreased in energy, i.e. *redshifted* by the the Universe's expansion,
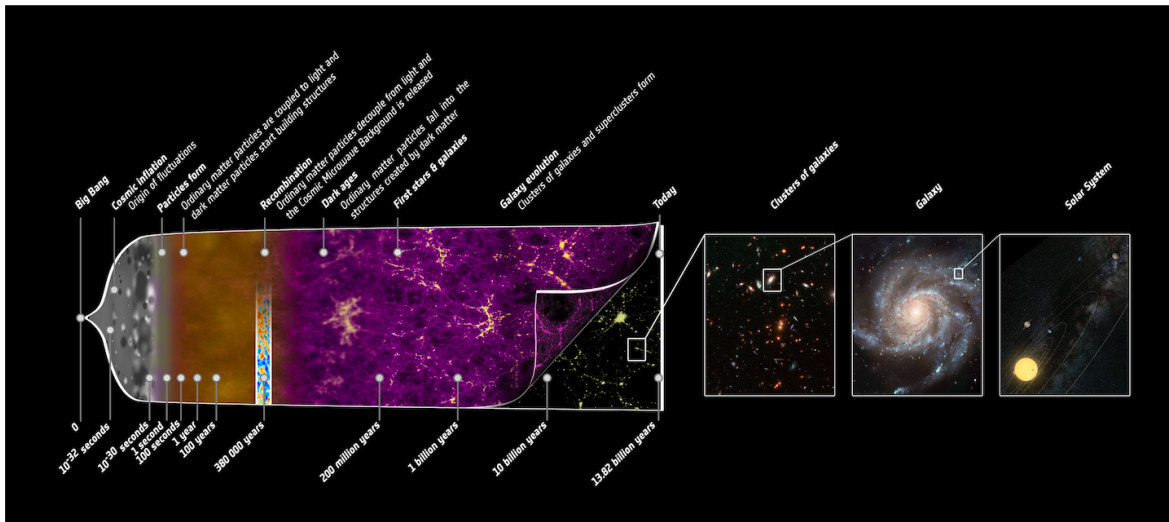
Figure 1.1: Illustration of the Universe's past. The purple overlay represents the dark matter structure, while the consequent stellar distribution is indicated in the image beneath. *Image credit*: ESA - C. Carreau (`www.esahubble.org`).

they still frame a remarkably precise and isotropic blackbody radiation with $T = 2.725$ K, only disturbed on small scales by tiny temperature fuctuations in the order of 10^{-5} (Planck Collaboration et al., 2020). While the baryons, i.e. the matter component which interacts with electromagnetic fields, were coupled to radiation, dark matter has not been tied in place by photons and thus already has began to flow into local overdensities, forming the very first structures. Now free to move, baryons plummeted into these gravitating dark matter halos. Filled with neutral gas, the Universe transitioned into the Dark Ages, since there were still no sources of light present. But eventually gas started to cool down, fragmenting into subclouds, which further collapsed and ultimately formed the very first, extremely massive stars – the so called Population III stars – reionzing the Universe. Thereafter collapsing and building subsequently larger structures, Cosmic Dawn marked the onset of a new era, which led to the formation and clustering of galaxies we observe today.

Starting from Einstein's field equations, Friedmann (1922) derived a set of equations, which allowed for a dynamically evolving Universe[1]. He used a dimensionless parameter to describe time dependant distances, which is now referred to as the time dependant scale factor $a(t)$. It relates the *proper* distance $r(t)$ at time t to the distance r_0 at a reference time t_0 and yields a time dependant recession velocity $v(t)$ for distant objects:

$$r(t) = a(t) \cdot r_0 \implies \dot{r}(t) = v(t) = \underbrace{\frac{\dot{a}(t)}{a(t)}}_{\equiv H(t)} r(t). \tag{1.1}$$

Such a relationship was later observationally confirmed by Hubble (1929), which is why the proportionality factor in Equation 1.1 for recession velocities measured today was called the Hubble constant H_0. Since its value is still subject of active research, it is usually expressed

---

[1]cf. Nussbaumer & Bieri (2011) for a concise review on the historical timeline.

in terms of the dimensionless parameter h as $H_0 = h \cdot 100$ km/s/Mpc. The discrepancy between results using different observational techniques (cf. Figure 1.2) is referred to as the Hubble tension and has nowadays initiated a debate on whether these disagreements can be traced back to observational errors or if it indicates the presence of yet unknown physics. If expansion would have been linear, the Hubble time $t_H = 1/H_0 \approx 14$ Gyr would be the age of the Universe. Although this is not the case, t_H is still widely used as an approximation to compare time scales, since the estimated true age is only "slightly" lower with 13.8 Gyr.
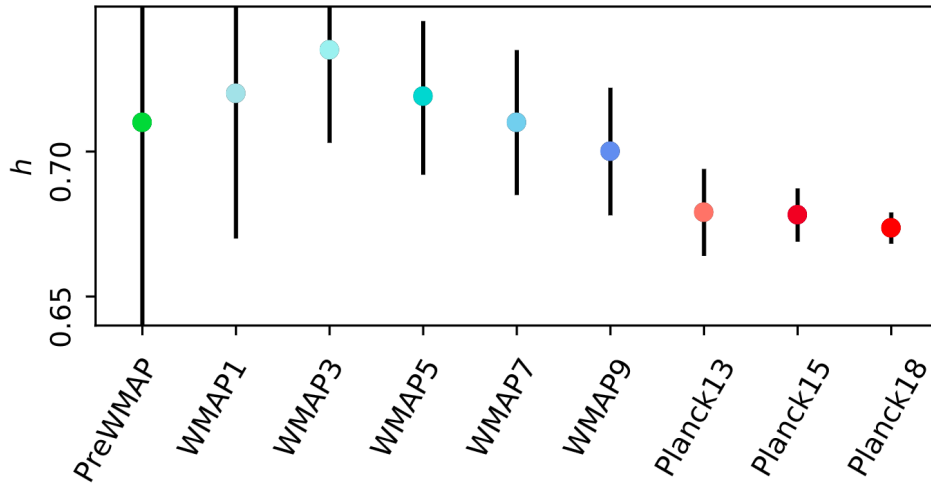

Figure 1.2: Fifth panel of Figure 12 by Planck Collaboration et al. (2020), demonstrating the disagreement between different missions measuring the dimensionless Hubble constant h.

While travelling through expanding space, the frequency of a photon is decreasing according to $\nu(t) \propto 1/a(t)$ (Binney & Tremaine, 2008), resulting in a larger, "redder" wavelength. Hence we can define the *cosmological redshift* z as the relative increase in the wavelength λ_o of a photon observed today, compared to its original wavelength λ_e when it was emitted at time t_e:

$$1 + z \equiv \frac{\lambda_o}{\lambda_e} = \frac{\nu_e}{\nu_o} = \frac{1}{a(t_e)}, \quad \text{since } a(t_0) = 1. \tag{1.2}$$

This relation motivates the usage of redshift z as a measure for elapsed time, rather than the "true" cosmic time, since the latter is depending on the applied cosmological model, while z can be directly measured by comparing wavelengths of observed lines to laboratory values.

1.2 (Modern) Talking about Structure Formation

Nowadays, the so called ΛCDM-paradigm is widely endorsed by the scientific community as the standard model for cosmology. The name encodes its two essential contributions, namely (a) an accelerated expansion of the Universe, driven by a yet unknown field, hence referred to as dark energy Λ and (b) dynamically **C**old **D**ark **M**atter. Growing hierarchically by accretion and mergers with nearby accumulations, halos continue to increase in their mass.

Since baryons contribute only a small fraction to the total matter content in the Universe, they follow the gravitational potential of collapsed dark halos, eventually condensing into stars and galaxies at their center. Hence light can be used as a tracer for the underlying dark matter distribution and reveals the gravitationally dominated Large Scale Structure. At least on large scales, such observations verify the notion of the cosmological principle – namely a homogeneous and isotropic Universe – and is also reproduced by cosmological simulations. However, our very existence is attributed to deviations from such a plain distribution. Gravitational collapse onto inhomogeneities led to the present Cosmic Web (cf. Figure 1.3), characterized by massive nodes called *galaxy clusters*. They are the most massive agglomerations of dark matter and galaxies and constitute the largest bound structures, which are continuously being fed by inflowing material from the interconnecting filaments. Enormous cavities with low densities in between these structures lead to the impression of a sponge-like appearance.
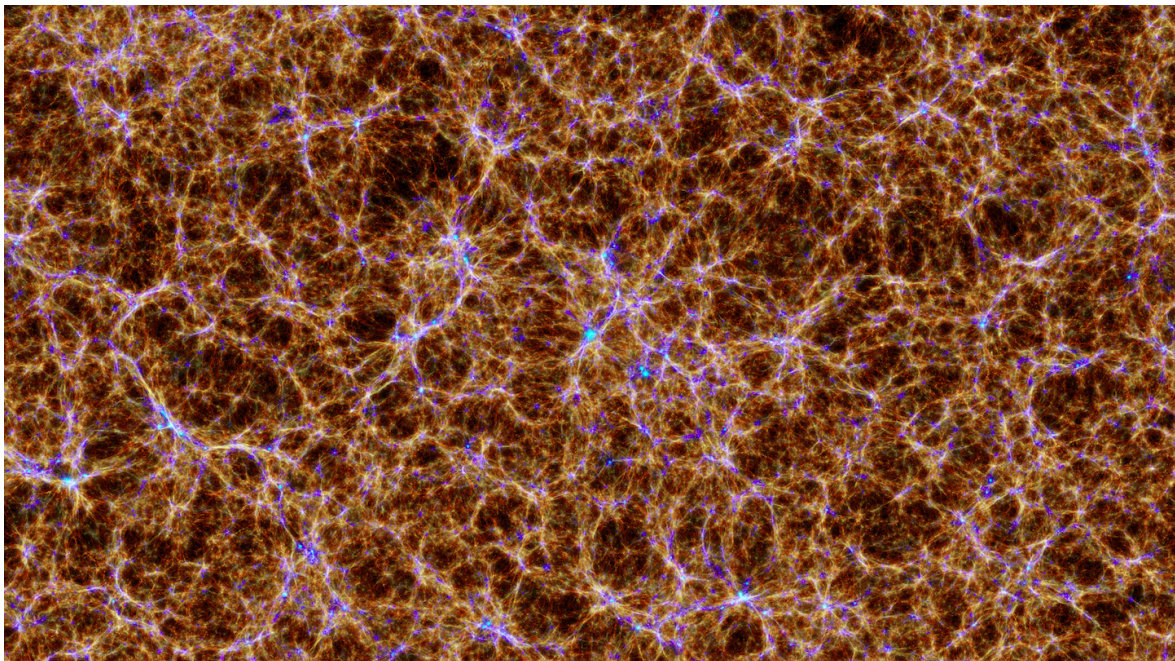

Figure 1.3: Visualization of the matter distribution in a cosmological simulation from the Magneticum pathfinder simulations (Box2b/hr). Brown and blue indicate cold and hot gas temperatures, respectively, while galaxies are colored in white. *Image credit*: Klaus Dolag (www.magneticum.org).

To characterize collapsed matter structures, naturally one will first try to assign masses, which would enable to compare them with each other. However this is not as straightforward in astrophysical context – where does one "object" end and where does the next begin? In principle, we are interested in the cumulative mass of *gravitationally bound* particles. But since the Universe is expanding, gravity is constantly competing against this oppositely directed force, pulling everything apart. Therefore a region needs to be sufficiently dense with respect to the background to detach from the omnipresent expansion and start collapsing. For this reason we can define the boundary of an object – and thereby also its enclosed mass – as the radial distance to its center beyond which the density undercuts a threshold. The value of this threshold depends on the underlying cosmological model. Nowadays it has

become common practice to parametrize it in terms of an overdensity Δ_c with respect to the so called critical density ρ_c, which would be the background in a spatially flat Universe with no curvature, assuming a FLRW-metric. In a flat and matter-dominated (Einstein-de-Sitter) universe, structures will collapse if they lie inside a density region with $\rho \gtrsim \Delta_{c,200} \cdot \rho_c = 200 \rho_c$ (Bryan & Norman, 1998). Hence we can define the approximate radius R_{200} of a structure as the spherical region which fulfils this condition, defining its corresponding mass M_{200} by counting the enclosed particles. Since these assumptions are very simplistic, the value of the applied overdensity Δ_c can vary across literature and is usually specified in the subscript of the radius or mass estimate. After detaching from the background, the system will eventually strive for virialization, i.e a dynamically steady state. Considering that only particles within these regions can be gravitationally bound and eventually collapse into a virialized structures, R_{200} and M_{200} are commonly referred to as the virial radius and mass, respectively, although their definitions are fundamentally different.

1.3 Properties and Evolution of Galaxies

In general, galaxies are classified according to their morphology. To this end, astronomers are consulting the so called Hubble sequence, proposed by Hubble (1936) and later extended by Sandage (1961). The associated types are typically aligned in a *tuning fork*-like shape (cf. Figure 1.4), hence earning the sequence its nickname. It distinguishes between four different classes: ellipticals (E), lenticulars (S0, SB0) spirals (S, SB) and irregulars (Irr).

Elliptical galaxies, also called early-types, display an amorphous appearance and are characterized according to their ellipticity $\epsilon \equiv 1 - b/a$, where b/a is their apparent axis ratio. Such a galaxy will be tagged as En, where the integer n is increasing for higher ellipticities ϵ. Their surface brightness falls off smoothly in their outskirts, without any clear boundary. Therefore, their sizes are typically defined as the distance from its center within which half of the object's total light is contained. This extent is then referred to as the half light-radius or effective radius r_e. The majority of elliptical galaxies is dominated by an old stellar population, which is attributed to gas deficiency and hence low interstellar medium (ISM) content, leading to a reddish color. Compared to the star formation activity of other types, ellipticals are usually quiescent. However, starburst episodes can happen even in early-type galaxies due to environmental interactions such as in a merger with a gas-rich galaxy (e.g. Hau et al., 1999). If an elliptical galaxy is large enough, it can ignite an *active galactic nucleus* around its central supermassive black hole – a comparably small but very bright accretion disk, emitting in all wavebands. Such massive ellipticals are often found in the center of galaxy clusters, surrounded by a dim stellar halo – the intracluster light (ICL) – reaching to the outskirts of the cluster. Due to their high luminosity compared to neighbouring objects, they are often referred to as *brightest cluster galaxy* (BCG) and are believed to form by hierachical assembly involving major mergers (Dubinski, 1998). Subjected to tidal torques in the giant halo of the cluster, stars are continuously stripped from galaxies, which then start to orbit independently
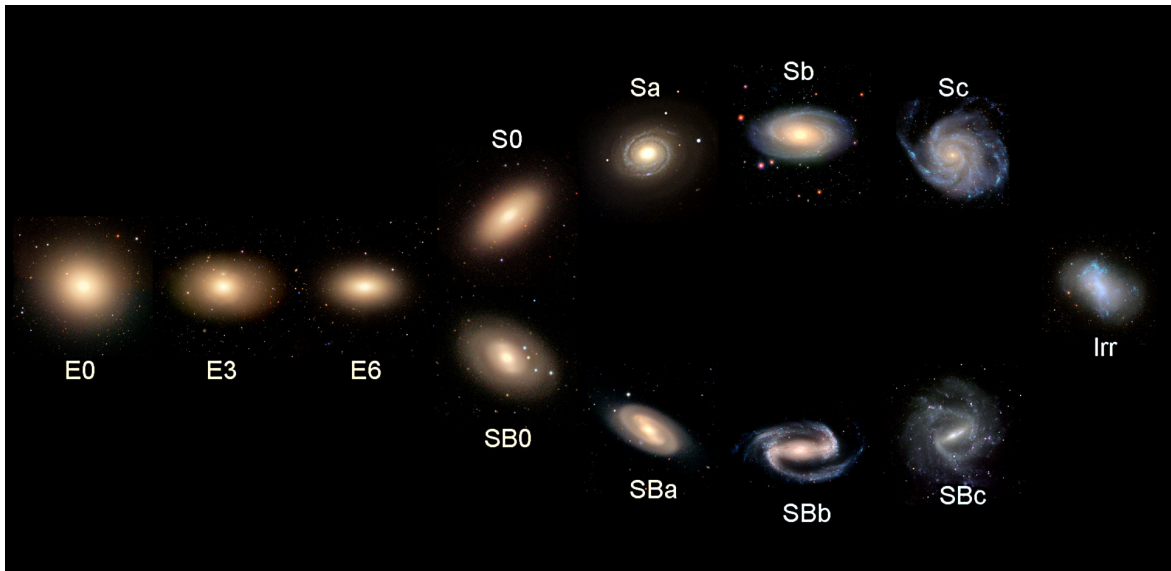
Figure 1.4: Galaxy classification scheme by Hubble and Sandage. *Image credit:* Zooniverse, ESO (`www.supernova.eso.org`).

and establish the ICL.

Spiral galaxies, also referred to as late-types, are characterized by their flat disk with eponymous features containing young stellar populations and dust lanes. The spirals are a consequence of a density wave moving through the disk's ISM, continuously triggering the formation of new stars along its way and granting them their bluish appearance. The central bulge is distinguished by an old stellar population and has an either spherical or barred shape – similar to ellipticals, albeit much smaller. According to this morphology, the spiral is labeled as S or SB galaxy with a spherical or barred bulge, respectively, while an ensuing small letter encodes the state of the spiral arms. In between the morphology of an elliptical and spiral galaxy, observations also find *lenticular* galaxies with stellar disks and bulges, but missing spiral features due to the lack of gas. It has been speculated that such galaxies could emerge from late-types by environmentally driven depletion of their gas content (van Gorkom, 2004). A key driver for this could be the intracluster medium (ICM), i.e. the hot gaseous atmosphere of galaxy clusters. Moving through this "sea" of gas, the ISM contained by a galaxy will experience a drag force called *ram pressure p*, which is describable by hydrodynamics and depends on the relative velocity v approximately as $p \propto v^2$ (Choudhuri, 1998). Such an effect can be observed in so called Jellyfish galaxies – disks falling face-on into clusters, thereby developing a trail of lost gas with distinct star forming knots (cf. Figure 1.5).

Ongoing star formation activity and subsequent stellar feedback in galaxies causes a continuous enrichment of their ISM with elements heavier than hydrogen and helium. The concentration of these constituents is commonly referred to as *metallicity* and serves as a tracer for the star formation history of both early-type and late-type galaxies. These terms are fossil from the initial hypothesis, that the former transition into the latter over time. In fact, it seems to be the opposite. Spiral galaxies form from accumulated gas in halos, which
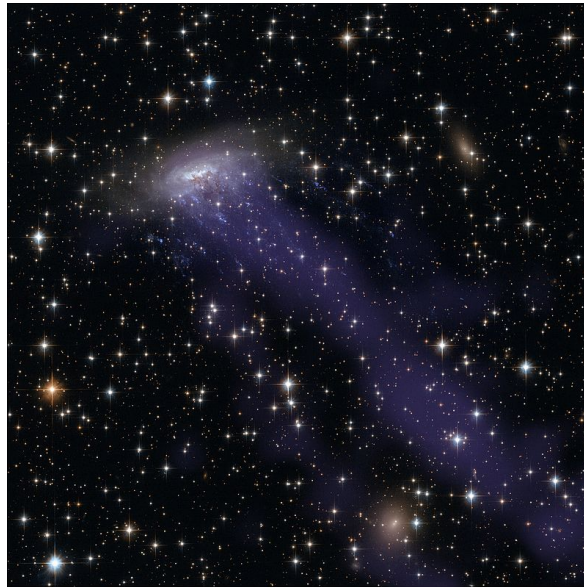
Figure 1.5: Combined image of ESO 137-001, using the Hubble Space Telescope (optical) and Chandra X-ray telescope. *Image credit*: NASA, ESA, CXC.

gradually cools and settles into a disk by redistributing its angular momentum and ultimately igniting star formation there. Elliptical galaxies, on the other hand, were demonstrated in simulations to assemble by mergers of spiral galaxies – a violent process, able to drive out the carried gas content (e.g. Gerhard, 1981; Burkert & Naab, 2003). Such *major mergers* – i.e. collisions between galaxies with comparable sizes – convert the orderly motion of stars into random directions, while the colliding gas is triggering star formation across the collisional debris. Such encounters of gas-rich galaxies are referred to as wet mergers, while the case of gas absence is called dry. The so called *irregulars* in the Hubble sequence are often the aftermath of a collision (e.g. shown in pioneering simulations by Toomre & Toomre, 1972), although they can also be caused by mere galactic flybys – or *galaxy harassment* – deforming galaxies in the resulting tidal field. But the most spectacular tidal features are produced by mergers, driving out material over length scales multiple times the size of the galaxies. Figures 1.6a and 1.6b display two beautiful examples of peculiar galaxies producing such structures called *tidal tails*, which are typically formed by encounters with relatively large impact parameters. However, if a disk galaxy collides face-on with another system, it can cause a rapidly expanding density wave in radial direction, causing a luminous ring of young stars around its progenitor (cf. Figure 1.6c). After settling down, such a radial merger can lead to shell-like traces around the galactic centre (Karademir et al., 2019) as e.g. in Figure 1.6d. Of course, mergers are not compelled to be binary interactions only, although they are more probable. Figure 1.6e shows Stephan's Quintet – a constellation of five galaxies appearing to be next to each other. In fact, "only" four of them are interacting, since NGC 7320 in the upper left is actually located much closer to Earth then the rest (Moles et al., 1998). Nevertheless it is still an impressive showcase for a multiple merger, likewise the triple merger IC 2431 (cf. Figure 1.6f).

Figure 1.6: Compilation of observed galaxies showing signs of interactions. *Image credit*: NASA/ESA (a) HST Robert Gendler (b) HST Holland Ford (c) CSA, STScI/JWST (d) HST Judy Schmidt (e) CSA, STScI/JWST (f) HST.
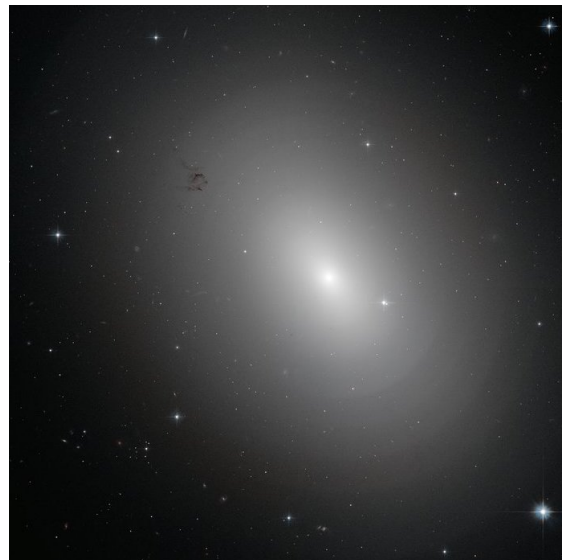

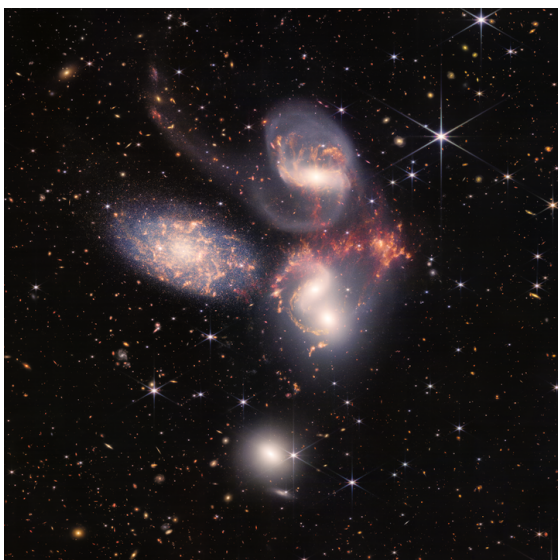**(a)** NGC 4038, NGC 4039 – "Antennae Galaxies"
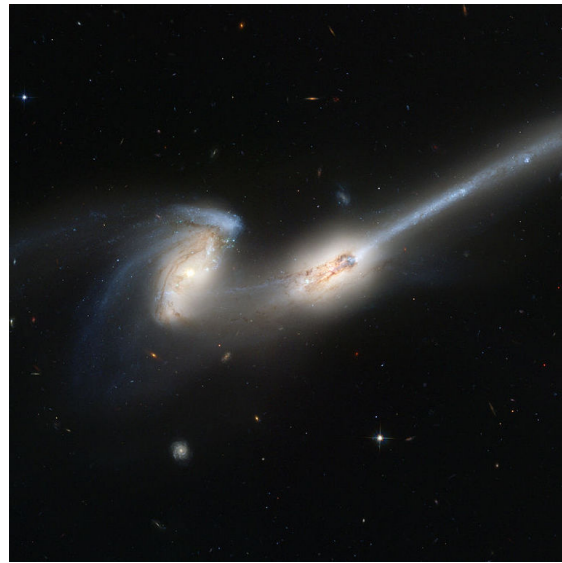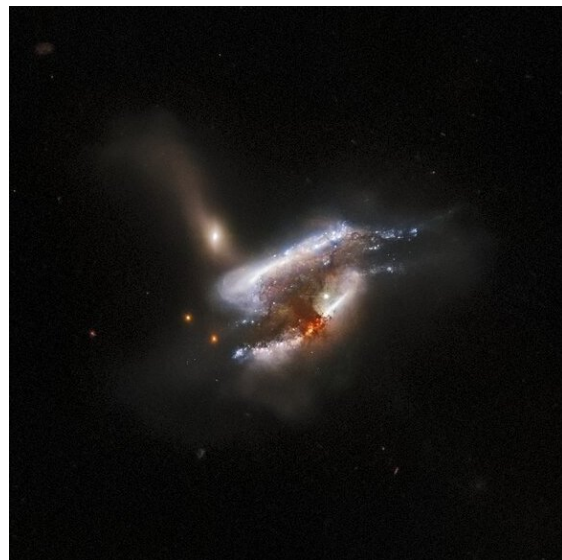

(b) NGC 4676 – "The Mice"

(c) ESO 350-40 – "Cartwheel Galaxy"

(d) NGC 3923

(e) "Stephan's Quintet"

(f) IC 2431

1.4 Dwarf Galaxies: Out of Sight, But Not Off Mind

The galaxies mentioned beforehand in context of the Hubble sequence typically have stellar masses of $\log_{10} M_*/M_\odot \gtrsim 10$. Such large masses also generate high luminosities, facilitating their discovery. The bulk of the total stellar mass, however, is carried by objects that are smaller than such "typical" galaxies. This was demonstrated by observations (Li & White, 2009; Baldry et al., 2012), as well as cosmological simulations through measuring the *stellar mass function* (cf. Figure 1.7). It is defined as the number density of objects per stellar mass bin and yields a dominating low-mass component in the low-redshift Universe.
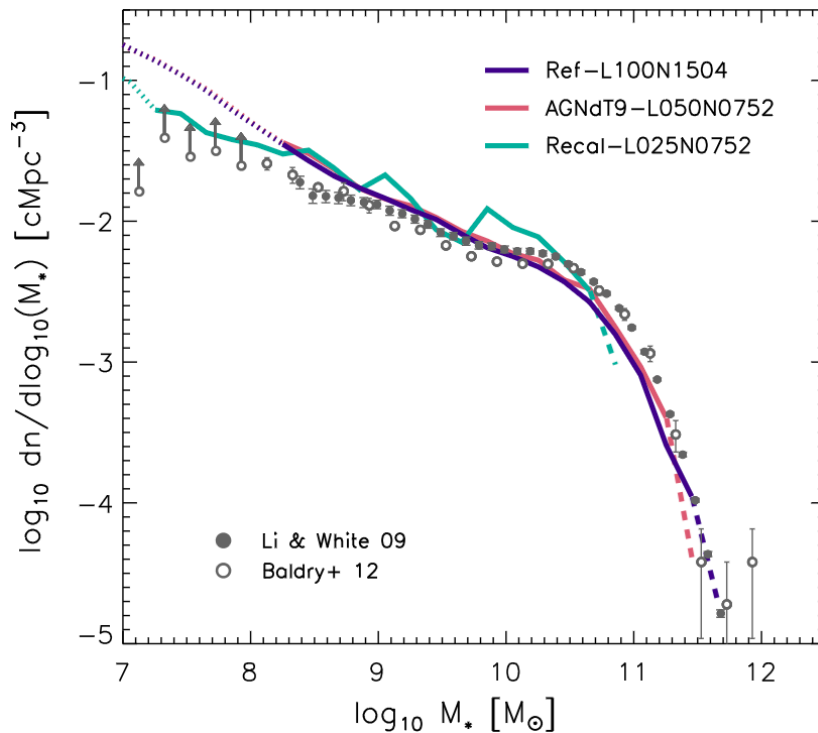

Figure 1.7: Figure 4 by Schaye et al. (2015), comparing the stellar mass function in their cosmological simulations EAGLE (lines) with observations (points) at $z = 0.1$.

Albeit their frequency, such *dwarf galaxies* are difficult to identify because of their low luminosities. Despite the challenge, observers have already found a diversity of dwarf galaxies, which can vary widely in their appearance and composition, posing riddles to their origins. Starting with dwarf ellipticals (dE) (Reaves, 1956), explorations found successively smaller objects, such as dwarf spheroidals (dSph), characterized by low gas content and an old stellar population. However not all dwarfs are quiescent systems, such as e.g. ultra-compact dwarfs (UCD), which display signs of active star formation in terms of high metallicities (Drinkwater et al., 2000). Since they are often located inside galaxy clusters (e.g. Mieske et al., 2004), it has been speculated whether UCDs could have formed through tidal stripping of larger galaxies (Kazantzidis et al., 2004). Another remarkable class is the ultra-diffuse galaxy (UDG), which was established very recently by van Dokkum et al. (2015). As the name suggests, such dwarfs exhibit extremely low luminosities, having large effective radii compared to other objects. Although it is generally challenging to estimate the dark matter

content of a distant galaxy – usually by inferring the total gravitating mass from velocities of orbiting stars – observations could still deduce the non-baryonic contribution of UDGs. Interestingly enough, they found dark matter fraction at both extremes, i.e. UDGs entirely dominated by a dark component (e.g. Gannon et al., 2020), but also similar objects nearly devoid of dark matter (e.g. Danieli et al., 2019).

1.5   Simulation Code GADGET-3

Simulating an astrophysical arrangement such as for example a galaxy or even a cluster of galaxies requires a computational method not only able to treat gravitational interactions, but also the dynamics of gas. Since the mean free path of gas particles is much smaller than the regarded length scales, we can rest upon the hydrodynamic equations to model their evolution. While hydrodynamic mesh codes operate by dividing the simulation volume into a grid and calculating fluxes between adjacent cells, a **S**moothed **P**article **H**ydrodynamics (SPH) code decomposes the domain in terms of "particles" representative for the local mass distribution. The time evolution of the system is then obtained by solving the hydrodynamic equations in lagrangian form for each particle. Physical properties at each point r_i can be retrieved by summing over the contributions of a specified number of neighbouring particles N_{ngb}, weighted by a radially symmetric smoothing kernel $W(|\mathbf{r}_i - \mathbf{r}_j|, h)$ (cf. Figure 1.8). The smoothing length h, i.e. the radial extent of this smoothing function, is estimated for each particle separately by counting the number of closest neighbours, until the confined volume accommodates N_{ngb} enclosed particles. Hence the smoothing length h decreases in regions with higher particle number densities.
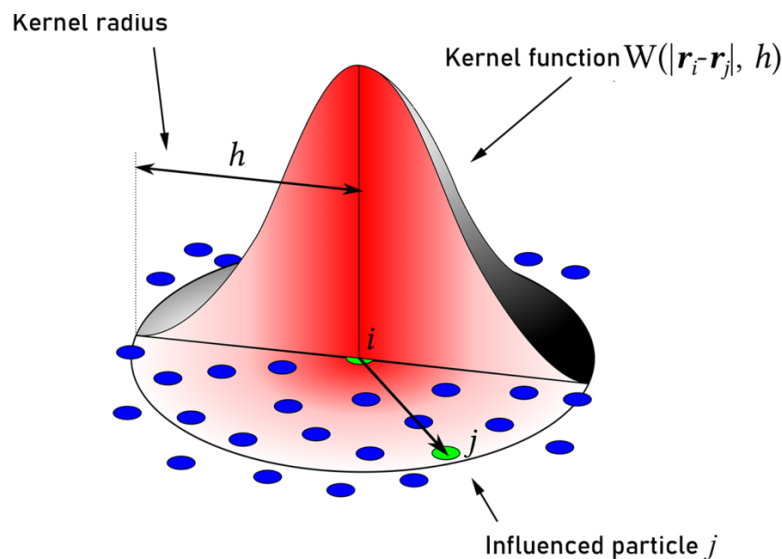

Figure 1.8: An illustration of the kernel function in 2D, centered at particle i with smoothing length h. *Image credit*: altered by Nghia Truong, Sreekanth Arikatla and Andinet Enquobahrie, originally licensed by CC BY-SA 4.0 (`www.creativecommons.org`).

The exact computation of the gravitational force acting on a particle in an N-body system would require to sum over each particle, resulting in $O(N^2)$ operations – an immensely expensive numerical cost for simulations involving a large amount of particles. Rather than considering the contributions of each particle separately, it would be more feasible to sample the gravitational field precisely in the vicinity of the particle of which we are trying to estimate the acting force, while disregarding the substructure formed by distant particles, summarizing their influence into one term. The *Tree method* proposed by Appel (1985) and Barnes & Hut (1986) is exploiting this idea. In such an approach, space is subsequently divided into volumes, until each subvolume encompasses at most one particle (cf. Figure 1.9). To calculate the net-force on a particle, the code performs a systematic "tree-walk": starting from the largest nodes (root), it checks whether it is sufficiently far enough away compared to the width of the node – or in other words, whether the solid angle of that node with respect to the particle is small enough. If so, then the mass inside that node is treated as a single particle located at its center of mass. Otherwise this process is repeated successively for its subvolumes until the tree-walk eventually reaches the smallest subunits (leafs) containing single particles.
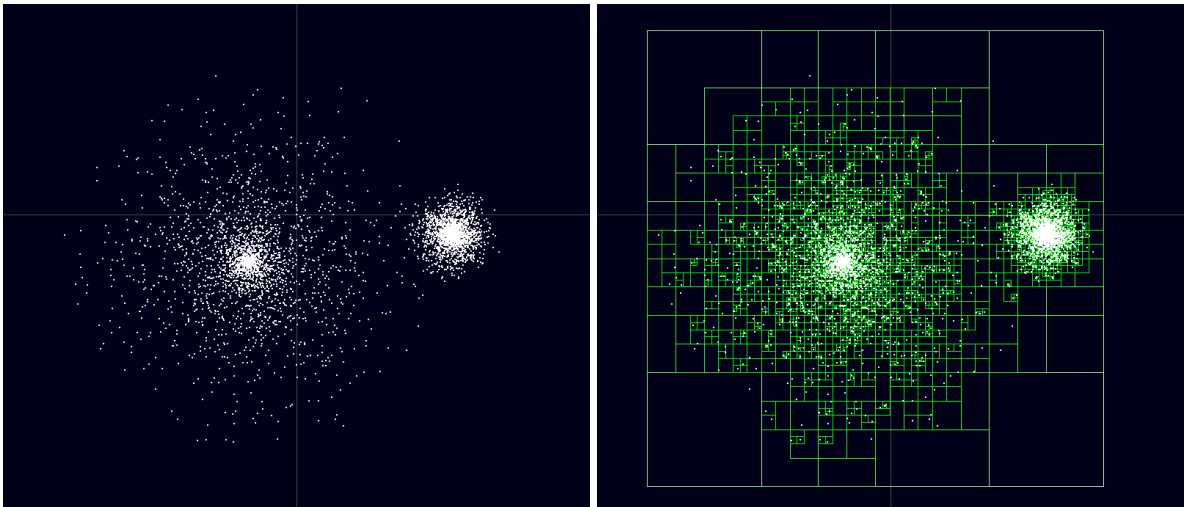
Figure 1.9: Demonstration of a Tree-algorithm. The targeted particle distribution is shown on the left, while the resulting domain decomposition is plotted on the right. *Image credit*: licensed by CC BY-SA 3.0 (`www.creativecommons.org`).

Large gravitational simulations like the ones described in this thesis cannot resolve each physical, "real" body, since the numerical workload would otherwise exceed the feasible limit. For example, each "stellar particle" in my simulations is actually representative for a whole stellar population. For this reason, I include a *softening length* in the evaluation of the gravitational force, to avoid unrealistic motions upon close encounters. The value for this softening length was chosen with respect to the calibrations of the galaxy merger simulations by Remus et al. (2013), scaling them according to my applied resolution.

All presented simulations were performed using the Tree-SPH code GADGET-3, which adopts the gravity force tree algorithm from its publically available predecessor GADGET-2 (Springel, 2005), but employs an improved SPH implementation by Beck et al. (2016), tackling shortcomings such as e.g. suppressed mixing in conventional SPH formalism (Agertz et al., 2007). In my simulations, I adopted a Wendland C2 kernel (Wendland, 1995; Dehnen & Aly, 2012), smoothing over 64 neighbouring particles. To reproduce a realistic astrophysical system, the code needs so called subgrid modules, which encode the physics occuring below the particle resolution. In particular, the code includes a star formation and supernova feedback model by Springel & Hernquist (2003), which treats the interstellar gas as a two-phase structure with cold, star-forming gas embedded in ambient hot medium. When the attributed density of a gas particle exceeds a given threshold, it is converted into a star particle, representative for a stellar isochrone population according to the initial mass function by Chabrier (2003). The code incorporates radiative cooling of optically thin gas in ionization equilibrium with an ultraviolet background (Katz et al., 1996). Supermassive black holes in the center of simulated galaxies are interacting with their surroundings via thermal feedback and are accreting gas according to the Bondi–Hoyle–Lyttleton model (Bondi, 1952), limited by the Eddington luminosity.

1.6 Project Idea in Context

Observations suggest that dwarf-sized galaxies contain a significant amount of mass in the galaxy mass function of the local Universe (e.g. Sabatini et al., 2003). Nevertheless, the variety of formation mechanisms and their respective contribution is still poorly understood. In particular, the presence of dark matter deficient galaxies reported by observations (e.g. van Dokkum et al., 2018, 2019; Guo et al., 2020; Mancera Piña et al., 2019; Hammer et al., 2020) raises the need to search for different evolutionary scenarios other than the typical halo collapse model. Clearly, it becomes crucial to consider the impact of the local environment and to study how external forces – namely tidal interaction and ram pressure stripping – could impact existing galaxies and thereby invoke the formation of different kinds of objects. In that context, there have been several mechanisms proposed, such as e.g. tidal stripping of the dwarf's dark matter component by a massive companion or a cluster (e.g Ogiya, 2018; Jing et al., 2019; Niemiec et al., 2019; Jackson et al., 2021), and separation between the baryonic and non-interacting dark matter component during high velocity collisions between several dwarf galaxies (e.g Silk, 2019; Shin et al., 2020; Lee et al., 2021; Otaki & Mori, 2023).

Another pathway discussed in the literature to produce dark matter deficient objects is the possibility of long-lived tidal dwarfs forming in the gaseous tails ejected by galaxy mergers (e.g. Mirabel et al., 1992; Bournaud & Duc, 2006; Bournaud et al., 2008; Kroupa, 2012). In such a scenario, structure formation would be triggered either by gas collapse due to Jeans instability or by local potential wells of ejected old stars, which in both cases induce further gas accretion, triggering star formation and ultimately the birth of a new gravitationally

bound and kinematically decoupled object (Duc, 2012). It is crucial to provide sufficiently large gas reservoirs to spark the formation of such star forming pockets, suggesting that at least one of the merging galaxies needs to have a high gas mass fraction (Wetzstein et al., 2007). Due to the inherent deficiency of dark matter at the tidal formation sites, such dwarf galaxies are expected to be dark matter poor (Barnes & Hernquist, 1992). Numerical studies of tidal dwarfs forming both in isolated mergers (Bournaud & Duc, 2006), as well as in cosmological simulations (Ploeckinger et al., 2018; Haslbauer et al., 2019) are able to recreate dark matter deficient tidal dwarf galaxies with a stellar population dominated by young stars. Observations find tidal dwarfs with such properties as well (Duc & Mirabel, 1998; Rakhi et al., 2023), such as e.g. in the vicinity of NGC 5291, shown in Figure 1.10. There are also cases reported with significant dark matter content or mixed stellar component though (e.g. Gray et al., 2023; Román et al., 2021; Kaviraj et al., 2012). However it needs to be stated that determining the tidal origin of dwarf galaxies in observations unambiguously is difficult, especially once the optical bridges between progenitor and dwarf disappear. Afterwards, the only established observational fingerprint to identify isolated tidal dwarf galaxies are unusually high metallicities, since their young stellar component is forming from ejected, pre-enriched gas (Duc, 2012). The presence of dwarf galaxies with deviant high metallicities for their luminosity in galaxy clusters (Poggianti et al., 2001; Duc et al., 2001; Iglesias-Páramo et al., 2003; Rakos et al., 2000) could signify a partly tidal origin, although different scenarios could also explain such peculiarities (Conselice et al., 2003b). Simulating the formation and evolution of tidal dwarf galaxies is challenging as well, since the necessity

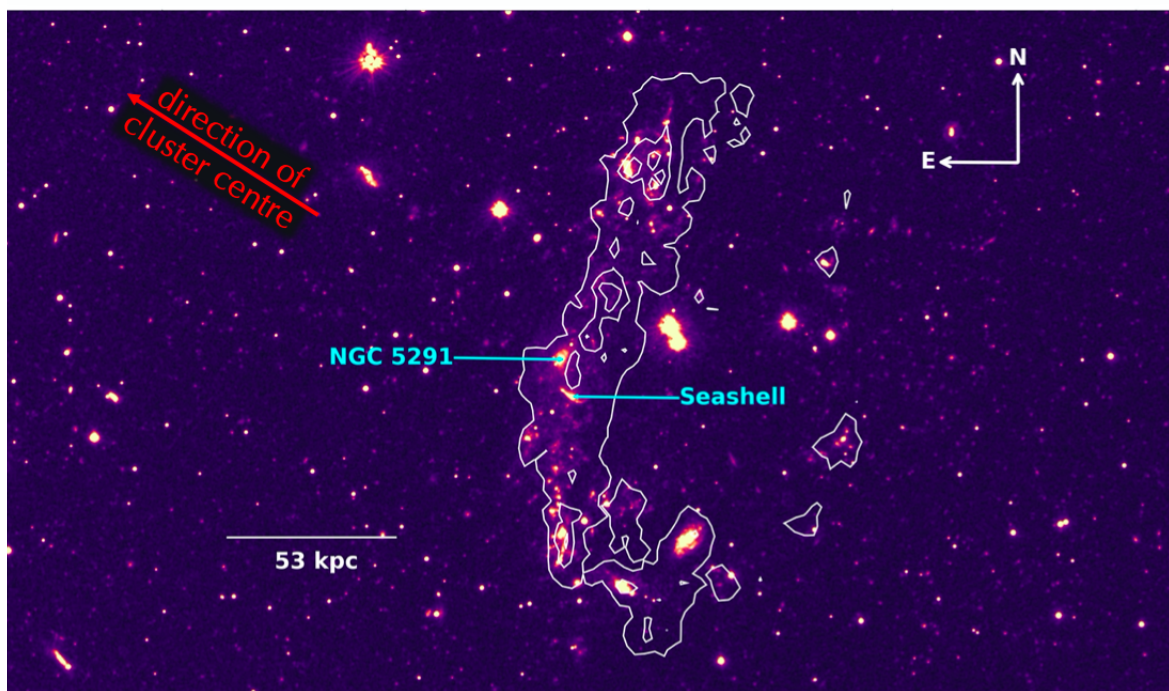**Figure 1.10:** Figure by Rakhi et al. (2023), showing the interacting galaxies NGC 5291 and the Seashell falling into cluster Abell 3574. Brighter color indicates higher flux in the near ultraviolet and hence also an increased star formation activity, while the white contours outline regions with constant neutral hydrogen density. The direction towards the clustercentric BCG is indicated by the red arrow.

to properly model gas fragmentation and succeeding star formation requires high resolution (Teyssier et al., 2010). In case of an included environment, e.g. the hot gaseous atmosphere of a galaxy cluster, it is therefore needed to resolve gas components of structures spanning over many orders of magnitudes in mass, driving up the numerical cost of the simulation. Nonetheless it becomes indispensable, as studies of single galaxies exposed to ram pressure already suggest a significant environmental impact by boosting the star formation activity, leading to Jellyfish galaxies (e.g Kapferer et al., 2009; Lee et al., 2022; Tonnesen & Bryan, 2021).

Both its location in the outskirts of a cluster, as well as convincing evidence for the presence of new stellar structures forming in its tidal tails (cf. Figure 1.10), frames the interacting system of NGC 5291 and the Seashell galaxy as an auspicious starting point to study the feasibility of environmentally driven formation of tidal dwarf galaxies. Moreover, such an arrangement prompts the intriguing question as to whether these newly formed stellar structures could even be stripped by the cluster, populating it with low-mass objects. The aim of my project was to model and test this possible evolutionary channel, utilising hydrodynamic simulations. I begin by studying the behaviour of isolated galaxy mergers in Chapter 2. Introducing the cluster in Chapter 3, I demonstrate that the environment is triggering a significantly enhanced star formation activity in the tidal features of a merger. After analysing the evolution of stripped tidal dwarf galaxies in Chapter 4, I discuss the implication of these results in Chapter 5 and provide an estimate for the tidal dwarf fraction among the total dwarf galaxy population. My conclusions are summarized in Chapter 6.

Big Boom Theory: Isolated Galaxy Mergers

"He who would learn to fly one day must first learn to stand and walk and run and climb and dance; one cannot fly into flying."[1] – it is a quite fitting description for this chapter. From the very beginning, the ultimate goal of my project was to test the behaviour of galaxy mergers in cluster environments. However, there were several stages which I needed to pass before I could *understand* simulations of colliding galaxies, because any other approach would have led to a merger between my project and a wall. Naturally, the first stage was devoted to setting up isolated galaxy mergers and to obtain a feeling for their behaviour, such that I could investigate the environmental influence later.

How does the respective orbit influence the morphology of the merger? At which distances to the progenitors is star formation even possible? Since I was interested in producing massive stellar structures in the tidal tails of a merger – i.e. *tidal dwarf galaxies* – it was clear that I would need to include a large gas fraction in the participating galaxies (Wetzstein et al., 2007). But could the extent of the gas reservoir have an impact on the behaviour? And what role would resolution play in such analyses? I needed to find answers for these questions. Therefore, this chapter is wholly dedicated to the study of isolated mergers. The general galaxy merger setup is explained in Section 2.1. In the subsequent sections, I describe relevant test cases and the resulting conclusions.

2.1 General Setup of a Galaxy Merger

The individual late-type galaxies participating in the merger were initialized using the method presented by Springel et al. (2005), which builds a stellar disc with associated cold gas mass fraction f_{gas}, a stellar bulge and a dark matter halo with a central black hole. The stellar and gaseous disc follow an exponential surface density profile given by

$$\Sigma_i = \frac{M_i}{2\pi l_i} \exp\left(-\frac{r}{l_i}\right). \tag{2.1}$$

---

[1]Friedrich Nietzsche

The subscript $i \in [*, \text{gas}]$ represents the stellar or gas component, whereas l_i and M_i denote the exponential scale length and total mass in the corresponding component. By default, both scale lengths (i.e. of the stellar disk and gas) have the same value.

Both the bulge and dark matter component are modelled by the spherically symmetric Hernquist profile (Hernquist, 1990)

$$\rho_k(r) = \frac{M_k}{2\pi} \frac{a_k}{r(r+a_k)^3}, \tag{2.2}$$

where the subscript $k \in [\text{b}, \text{dm}]$ denotes the bulge or dark matter component, while a_k and M_k are the scale length and total mass of the respective halo. In default mode, the scale length of the bulge is parametrized in terms of the disk scale length to $a_\text{b} = 0.2l_*$. In case of the dark matter component, the Hernquist distribution was selected since its total mass converges and associated analytical distribution functions allow an easier implementation than an NFW profile (Navarro et al., 1997). To not lose touch with common descriptions of haloes in cosmological simulations, M_dm is set to be equal to the mass enclosed within r_{200} in an NFW profile with matching central density, i.e. $\rho_\text{NFW} = \rho_\text{dm}$ for $r \ll r_{200}$, where r_{200} is the radius at which the mean enclosed dark matter density is 200 times the critical density of the Universe. Using this condition, the scale length a_dm is determined by the NFW concentration parameter c through Eq. 2 in Springel et al. (2005), which is set to $c = 12$ for all disk halos.

Figure 2.1 depicts an examplary initial condition of a galaxy with a total mass of $M_\text{tot} = 2 \times 10^{11}\ M_\odot$ and gas mass fraction in the disk of $f_\text{gas} = 0.2$. In this case, the particle resolution is equal for all components, namely $m = 3 \times 10^6\ M_\odot$. Dark matter is not included in this illustration, since it would dominate the whole field of view. It is worth to note that the isotropic sampling of the bulge (plotted in red) causes visible outliers in the outskirts of the galaxy. However, this inconsistency with respect to real galaxies is entirely negligible, since these stars constitute an insignificant fraction of the total stellar body and the whole object is surrounded by spherically distributed dark matter particles anyway.

After initializing the galaxies, I used a routine provided by Karademir et al. (2019) to create a merger configuration. The initial separation between the galaxies, as well as their impact angle and orientation of the disks are free parameters. Their relative velocity is set to $\Delta v = r_{200}/t_\text{ff}$ parallel to the x-axis, where r_{200} is the virial radius of the larger galaxy and t_ff the associated free-fall time in its spherically symmetric potential.[2]

---

[2]For reference, the value of Δv is similar to the respective virial velocity v_{200}.
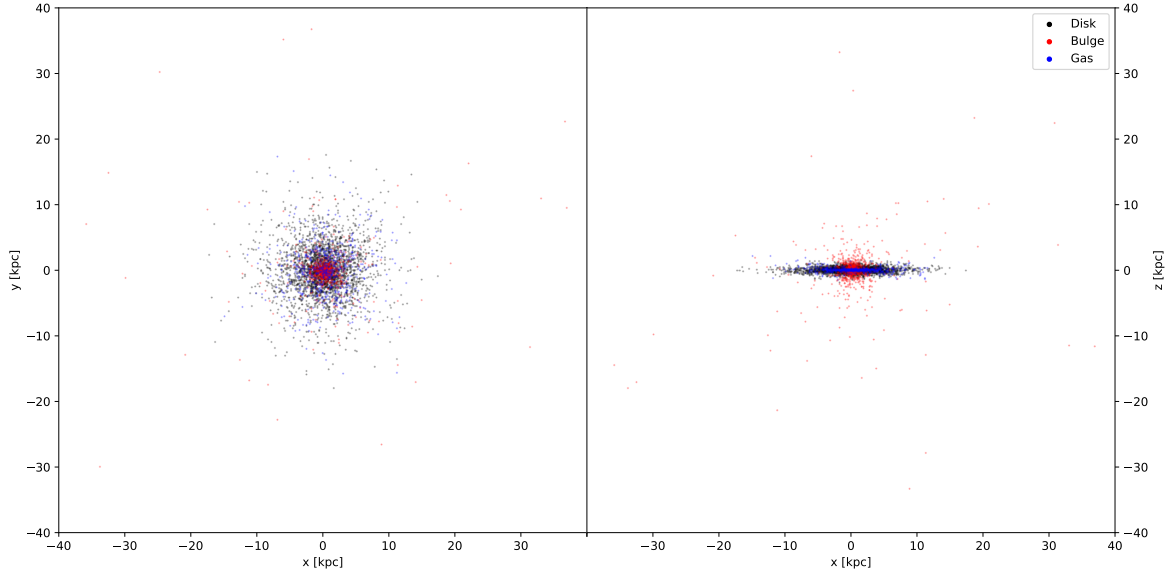
Figure 2.1: Initial condition of a late-type galaxy with total mass of $M_{\text{tot}} = 2 \times 10^{11} \, M_{\odot}$ and resolution $m = 3 \times 10^{6} \, M_{\odot}$.

2.2 Testing Various Orbits

In the beginning, particular focus was on reproducing the general merger features between NGC 5291 and the Seashell galaxy, observed in the cluster Abell 3574 (cf. Figure 1.10). After finding such a merger configuration, one could then later place it in a cluster environment and meet predictions about the fate of the observed object by analysing the simulation outcomes. Thus, I searched for configurations, which could simultaneously reproduce the following two morphological features:

(a) Far extended tidal arms in both directions

(b) Two merging stellar nuclei in the centre with different sizes

Before fine-tuning the individual galaxies, I first tested what general morphological differences one could observe by varying the orbits in a 1:1 galaxy merger. The first column of Figure 2.2 displays the initial conditions of four different configurations, while the second and third column illustrate their respective time evolution. The impact angle and relative orientation of the disks are the only difference between each scenario, while the initial separation is constant at 60 kpc. Each participating galaxy has a total mass of $M_{\text{tot}} = 2 \times 10^{11} \, M_{\odot}$, while the gas mass fraction in the disk is at $f_{\text{gas}} = 0.2$. This corresponds to about 15% of the total baryonic component. Gas is plotted in blue, whereas the black and red markers are tracing stars which initially belonged to the disk and bulge component, respectively. New stars forming from the gas after the beginning of the simulation are drawn in yellow. In the following, I summarize the main conclusions for each orbit.
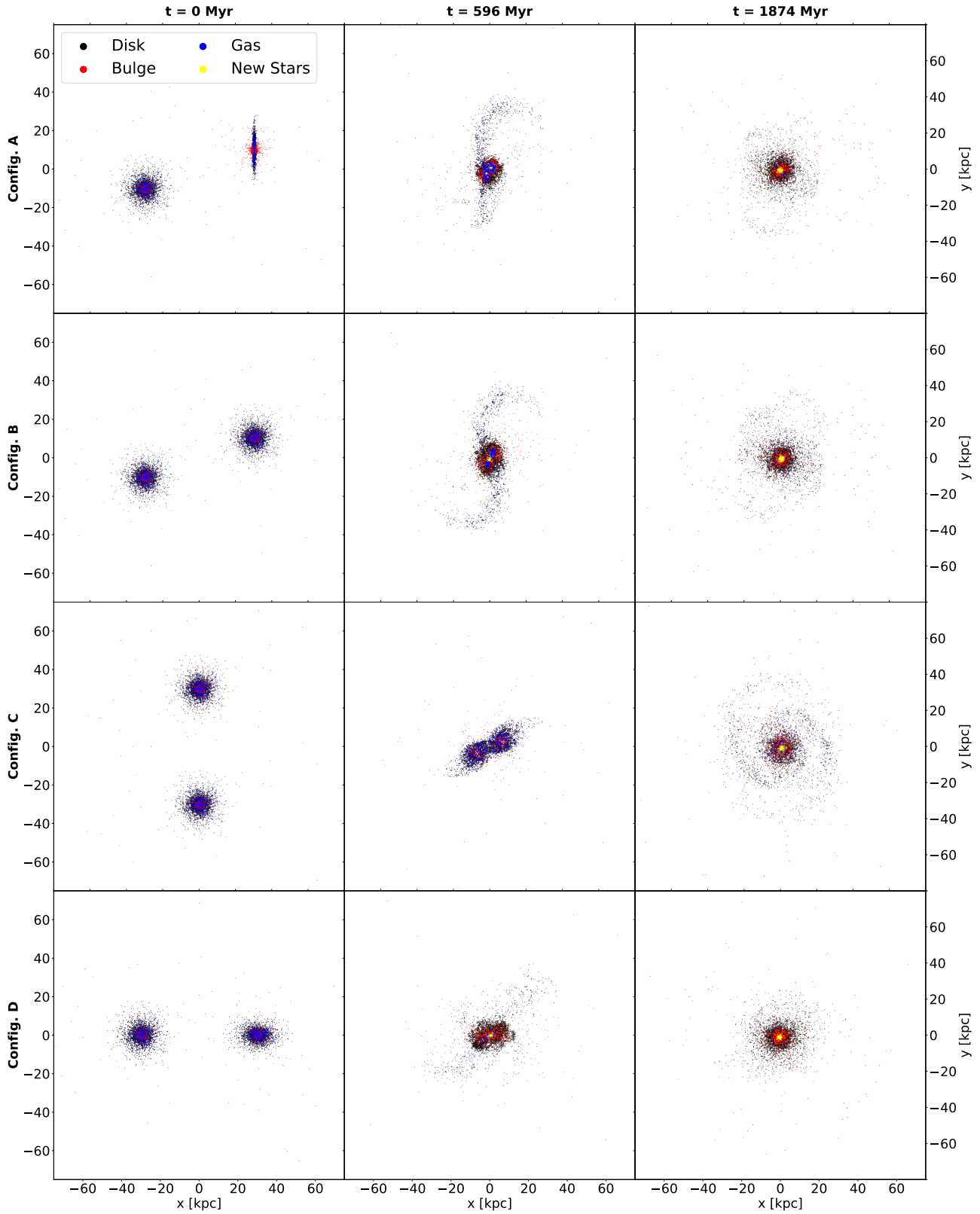
Figure 2.2: Morphology evolution test of four different configurations for a 1:1 major merger. Each galaxy has a total mass of $M_{\mathrm{tot}} = 2 \times 10^{11}~M_{\odot}$ and resolution $m = 3 \times 10^{6}~M_{\odot}$ per particle.

- *Config. A*: Implementing an **a**symmetric disk constellation unsurprisingly also leads to irregular tidal features. The two disks have a relative angle of 90°, while the impact angle with respect to their velocity is 20°. Since the total spins of both galaxies are not aligned, the tidal tails are not forced to be symmetric in both directions (with respect to the plotting plane). Thus, we see only one dominant tidal tail, while the other is less pronounced. Simultaneously, there are two distinguishable stellar cores in the merger centre visible (middle panel). At later stage, the remnant develops the morphology of a lenticular galaxy.

- *Config. B*: Since their disks lie in the same plane, the galaxies behave like **b**allet dancers – symmetrically and on-edge. The spins of both galaxies are aligned and as in config. A, they initially move under an impact angle of 20°. Momentum conservation causes the formation of two equally sized tidal tails, which in unison display a characteristic S-shape. Although there is separation of gas occurring in the centre after first close-passage, only one large stellar nucleus is produced by this configuration. Afterwards, the remnant settles to a late-type galaxy, while the collapsing tidal tails leave their imprint as faint spiral features. This is particularly interesting, since in the literature major mergers are generally expected to form early-type galaxies as their final remnant.

- *Config. C*: Set on a **c**ircular orbit by an impact angle of 90° with aligned disks, this merger displays similar features as configuration B, although on a larger timescale. Here, it takes more time to reach first close passage between the galaxies due to the increased impact parameter. Therefore, the tidal tails are not visible yet (third row, middle column), while these features are already in full blossom in the case of a smaller impact angle (second row, middle column). The tidal arms are winding up in the following development and lead to spiral features, which are still dominant almost 2 Gyr after the beginning of the simulation.

- *Config. D*: Finally, I tested a radial merger, where the disks are twiste**d** against each other by an angle of 45°. Upon impact, we can see traces of shells forming around the merging core, while also exhibiting two mildly pronounced streams in opposite directions. After settling down, the remnant reaches an equilibrium morphology, which resembles an early-type galaxy.

In general, my simulations reproduced the result of the merger studies performed by Karademir et al. (2019). Specifically, impact angles above a certain threshold produce tidal tails, whereas mergers with smaller collision angles are displaying shells as their dominant feature. Regarding my search of a suitable merger constellation to reproduce NGC 5291, three candidates exhibit at least one of the two criteria set above: A, B and C. Although the asymmetric configuration A is able to produce two distinct stellar nuclei, it does not form extended streams in both directions. On the other hand, B and C develop dominant tidal tails but do not display two distinct merging nuclei simultaneously. Since A and B only differ in the orientation of the disk plane, I chose to continue my tests with these configurations. Hence, to improve the similarity to the observed galaxy merger NGC 5291, I left the initial

orbit study with two hypotheses:

(i) To form two distinct stellar nuclei in the centre, I would need a merger ratio different from 1:1, since symmetry caused equally sized cores in this sample.

(ii) Developing further extended tidal tails may be possible by implementing more massive galaxies in the merger, as well as by increasing the initial separation or impact angle.

2.3   Changes With Resolution

Figuratively speaking, each particle in a SPH formalism represents the collective mass distribution around its position. Sampling the total distribution with more particles naturally decreases each of their masses, which in principle enables to resolve less massive structures in the simulation. Figure 2.3 compares the morphology of galaxy mergers in two different resolutions about 850 Myr after the beginning of the simulation. The left-hand side shows a merger between two disks having a relative angle of 90° (Config. A in Figure 2.2), whereas on the right-hand side both disks are initially aligned in a plane (Config. B in Figure 2.2).
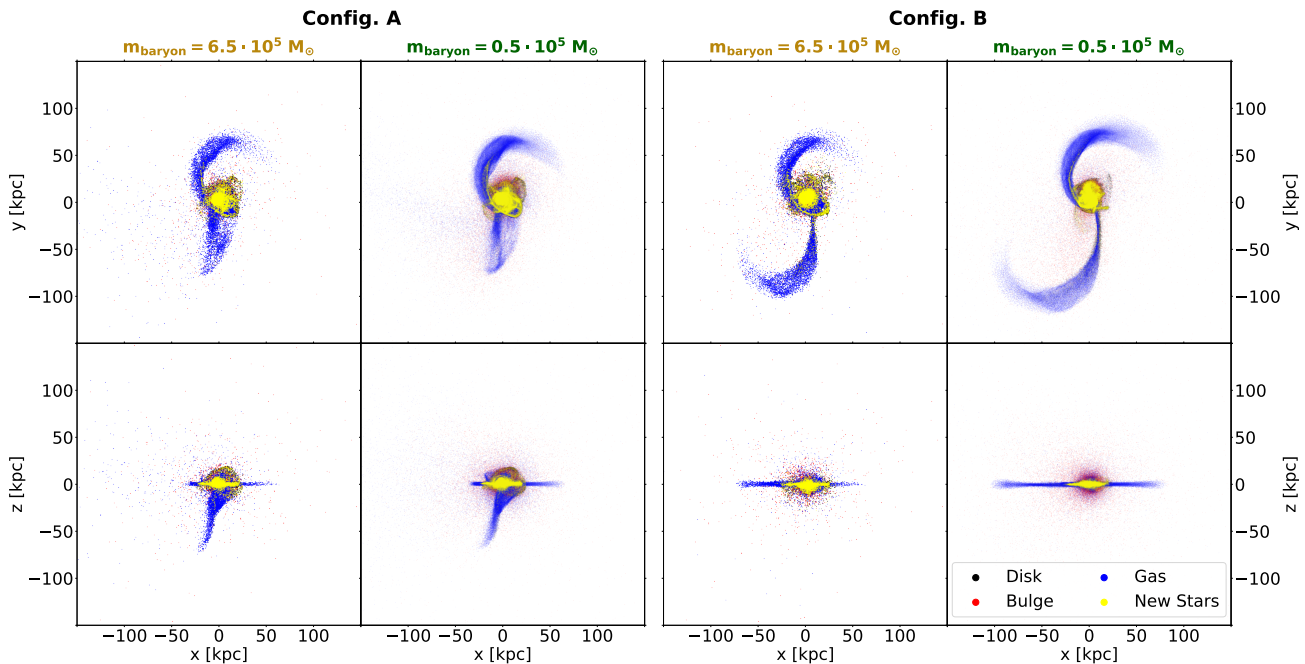

Figure 2.3: Comparison of merger morphology in two projections for config. A and B (cf. Figure 2.2) with varying resolution. The marker opacity for the improved resolution is decreased accordingly.

Compared to the tests in Section 2.2, I changed the mass ratio of the merger to 2:1 and increased the initial separation, as well as the mass of each participant. Thus, the larger and smaller galaxy now have virial masses of $M_{200,\mathrm{a}} = 1.4 \times 10^{12}\,M_\odot$ and $M_{200,\mathrm{b}} = 0.7 \times 10^{12}\,M_\odot$, respectively, and are initialized with a relative distance of 120 kpc. The left column for each of the two configurations shows a simulation with $m_{\mathrm{bar}} = 6.5 \times 10^5\,M_\odot$ per each baryonic particle (i.e. stars and gas), while the right column displays the exact same system, but with ~10x higher resolution. Obviously, both runs in each configuration reproduce a similar

morphology. Substructures and density gradients, however, are more pronounced in the cases with higher resolution – especially for the gas component. Hence we can trace the low-density regions at the tip of the gaseous tidal tail more accurately by sampling the volume with more particles.

During my project, I am ultimately interested in the formation of dwarf galaxies in the tidal features of a merger and their evolution with time. We already see in the isolated test cases studied in this chapter, that there are stellar structures accumulating in the high-density regions of the gas tails. However, they do not survive for longer than a few 100 Myr after their formation, since all extended tidal features are destined to fall back into the potential well at the centre due to lacking external influences. The hypothesis is that – upon placing the merger into a cluster environment – it might be possible to strip tidal dwarfs from their progenitor, which would unlock a new evolutionary channel towards the formation of dwarf galaxies. To maximize the chances of a stripping event, the merger itself needs to provide favorable conditions, namely the formation of massive stellar substructures far enough away from the merger center, such that the cluster is able to snatch them from their parents. Apart from finding such an advantageous merger configuration, resolution may play a role in simulating such structures as well, since a decreased particle mass might enable to model gas cloud fragmentation and cooling on smaller scales, possible leading to an increased stellar component forming during the interaction.

To study the impact of resolution on the formation of tidal dwarf galaxies, I compiled a histogram of the radial distance at which new stellar particles formed in the tidal tails of configuration A in Figure 2.4, where orange bars indicate the run with lower resolution, while the simulation with higher resolution is plotted in blue. The number of counts is cumulative up until the moment of the snapshot shown on the right-hand side, ~850 Myr after the beginning of the simulation. The tidal region used for the compilation of the histogram on the left-hand side is plotted in red. To extract the tidal tails, I applied two simple conditions: the particles needed to have a minimum distance of 20 kpc to the closest of the two present black holes, while also being in a region with high gas density above some threshold value. The former requirement avoids contamination by the galactic center, while the latter prevents counting of low-density material surrounding the site almost isotropically after the merger.

Although there are much more stellar particles forming with increasing resolution due to decreasing mass per particle, we can see in the plot below the histogram in Figure 2.4, that the integrated stellar mass per radial bin remains approximately the same. Hence this "low" resolution is already high enough to properly resolve gas fragmentation. Sampling with more SPH particles will only increase the numerical cost without allowing to resolve additional relevant substructures. Repeating the same procedure for configuration B does not lead to qualitatively different results, as we can see in Figure 2.5. Curiously, there is even a slight increase in integrated stellar mass in the case of lower resolution for radial distances between

30 kpc and 40 kpc. However, this is equivalent to only a few particles in the simulation and thus does not present a robust statistical difference.
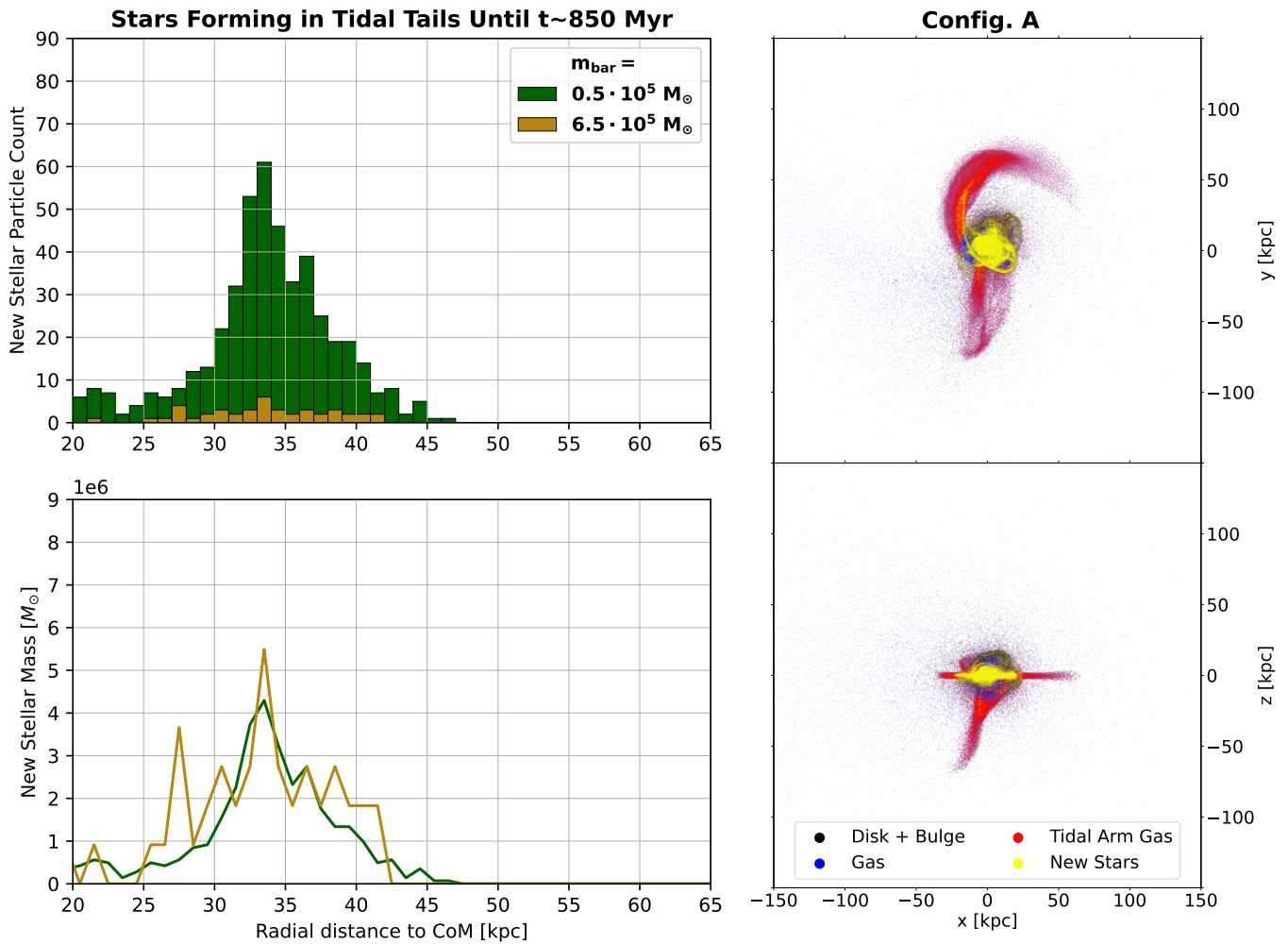

Figure 2.4: Star formation in tidal tails against radial distance to centre of mass (CoM) for config. A.

By comparing the histograms of the two different merger setups with each other, we can notice that configuration B produces more total stellar mass in the tidal features, as well as farther extended stellar tails. The "frontal" collision in configuration A leads to larger dynamical friction, since the material cannot move away from the merging centre after first close passage as smoothly as in the other setup. In configuration B, on the other hand, the aligned spins of the galactic disks lead to two dominant tidal tails by force of symmetry, enhancing the chances of forming new stellar structures. Therefore, this study highlighted configuration B as a promising candidate for future simulations involving environmental effects, since it provides more favorable conditions for tidal dwarf galaxy formation.
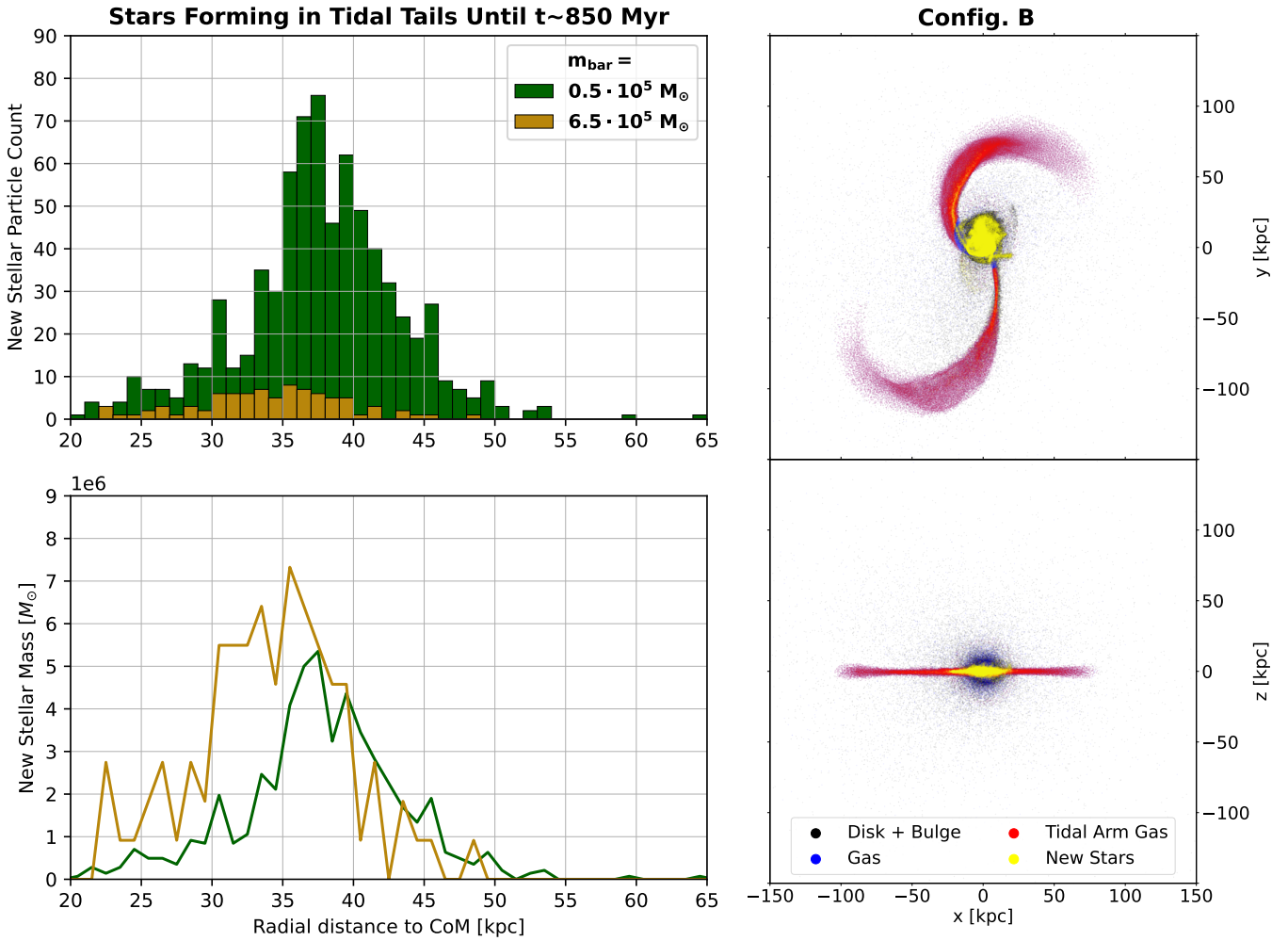
Figure 2.5: Star formation in tidal tails against radial distance to centre of mass (CoM) for config. B.

2.4 Impact of Galaxy Properties

At this point, I have tested the impact of orbit and resolution on the capacity to provide favorable conditions for tidal dwarf galaxy formation. Naturally, the next step is to investigate the influence of the individual galaxy properties on the merger morphology. In particular, my attention was focused on the role of the gas component, since new star structures can only be built from it in the first place. Hence it is necessary to provide a large gas reservoir in the merger, which is able to nourish the star formation pockets in its tidal tails, to ultimately produce a high number of dwarf galaxies after the impact (e.g. Wetzstein et al., 2007). Meanwhile, the extent of the cold gas disk could influence the morphology of the tidal features as well, since the position of a gas particle impacts how far it can be ejected by the interaction. Observations found neutral gas in galaxies to be much further extended than the stellar disk (e.g. Briggs et al., 1980; Martin, 1998), which motivates to test larger gas disk radii as well.

Figure 2.6 demonstrates morphological differences, which develop by varying the galaxy properties in the merger, while the geometrical arrangement remains constant at configuration B (cf. Section 2.2). The upper tile indicates the initial condition for each configuration,
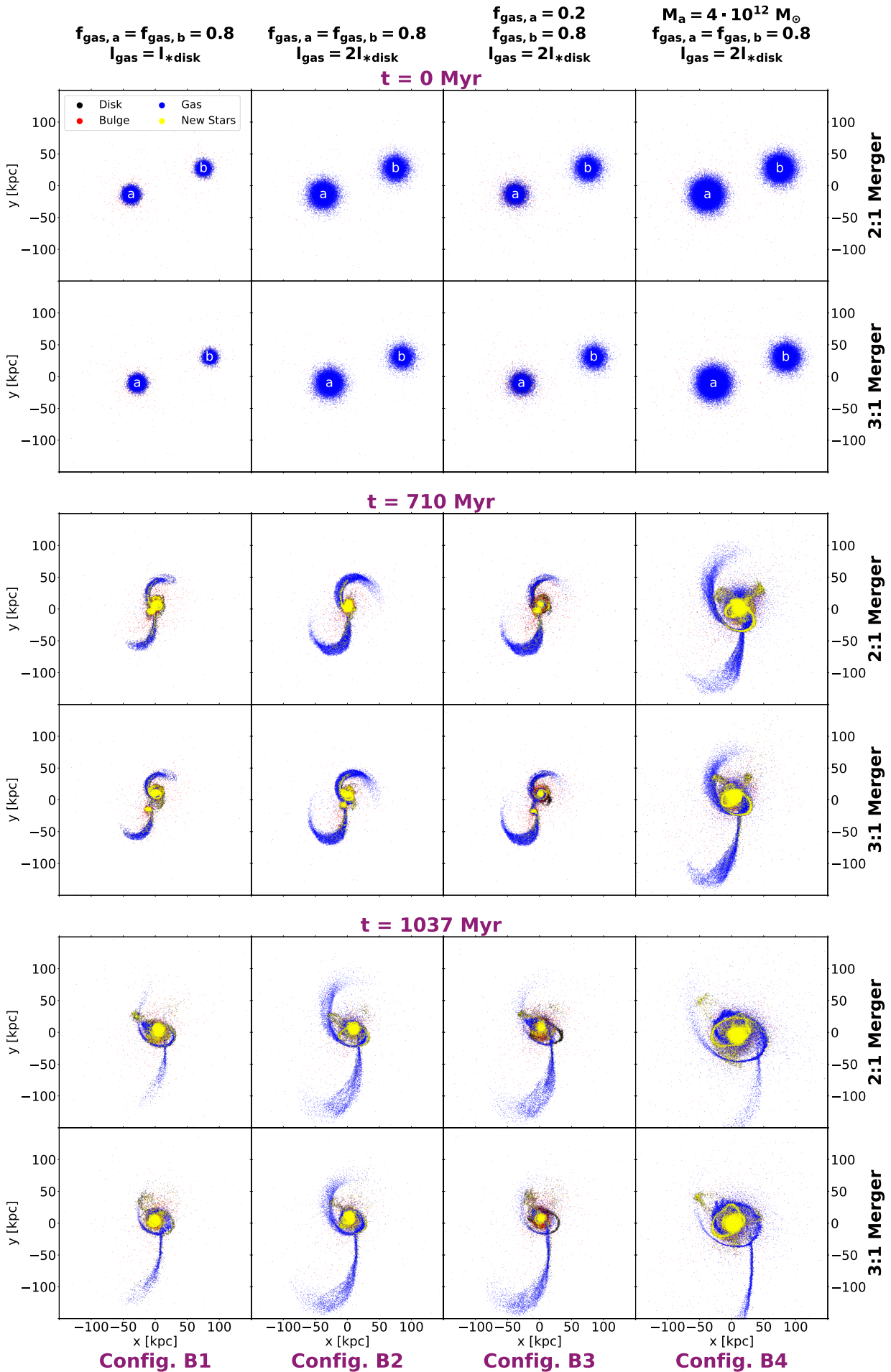
Figure 2.6: Morphological differences arising by implementing different galaxy properties.

whereas the two tiles beneath show the merger state at two different times. Each of these tiles has two rows, which display a 2:1 and 3:1 in the upper and lower row, respectively. Above each column, I list the attributes which specify the properties of the initialized galaxies. The baryonic resolution for each simulation is at $m_{\mathrm{bar}} = 6.5 \times 10^5 \, M_\odot$, since I have found this value to be sufficient to properly resolve star formation (cf. Section 2.3). The same compilation, but implementing the geometrical orbit of configuration A, is supplemented in the Appendix (Figure A1).

In the first three test cases – i.e. B1-3 – I implemented a galaxy with Milky-Way like virial mass of $M_{200,a} \sim 10^{12} M_\odot$ as the more massive progenitor, while varying the gas disk size and mass in the different configurations. Comparing the development between setup B1 and B2 illustrates the impact of the gas disk extent. Both mergers have an equally massive gas reservoir, but in B2 the gas in each galaxy is distributed across a larger disk with twice as high exponential scale length l_{gas} (cf. Equation 2.1) than in B1. This circumstance leads to longer and wider tidal tails in B2, which are both still clearly distinguishable ~1 Gyr after the beginning of the simulation. Introducing different gas mass fractions for both galaxies also leaves an imprint on the morphology, as we can see in configuration B3. Here, the more massive collision partner provides a smaller gas mass reservoir than compared to setups B1 and B2, which restricts the gas amount being able to be ejected by the merger. As a side note, the resulting asymmetry in the tidal tails poses as a demonstration of "division of labor" between the interacting galaxies – clearly, the smaller gas tail originated from the gas-poorer galaxy, while the tidal sibling must have built up from the gas-rich galaxy, since the tail is indistinguishable from its equivalent in B2. Finally in configuration B4, I increased the galaxy masses by a factor of ~3 compared to setups B1-3, while the other parameters are set as in B2. In this case, first close passage between the central black holes happens sooner – since their relative velocity is higher – and leads to a spectacular morphology with enormous tidal features. Such massive galaxies, however, are quite rare and the total mass of this complex is exceeding the observed comparison merger between NGC 5291 and the Seashell galaxy anyway. Regardless, I decided to include this setup in my compilation to illustrate the effect of altering the total galaxy mass, but also as eye-candy for the diligent reader.

Thus we have ascertained that a larger gas disk also leads to farther extended gaseous tidal tails. But is that also the case for the stellar component? By a short look on Figure 2.7 we can confirm this supposition. Here I count the number of stellar particles per radial bin and distinguish between the old star population originating from the bulge or disk and new stars formed since the beginning of the simulation. The moment for this snapshot is at $t \sim 850$ Myr, when the tidal features of the merger are much pronounced (cf. Figure 2.3). The left-hand side shows the case with small gas extent (B1), while the right-hand-side displays the exact same merger but with larger gas disks in the initialized galaxies (B2). Naturally, the majority of new stars in both configurations is close to the merger centre. In the outskirts, however, we can distinguish a clear trend towards larger radial distances reached by new stars in the
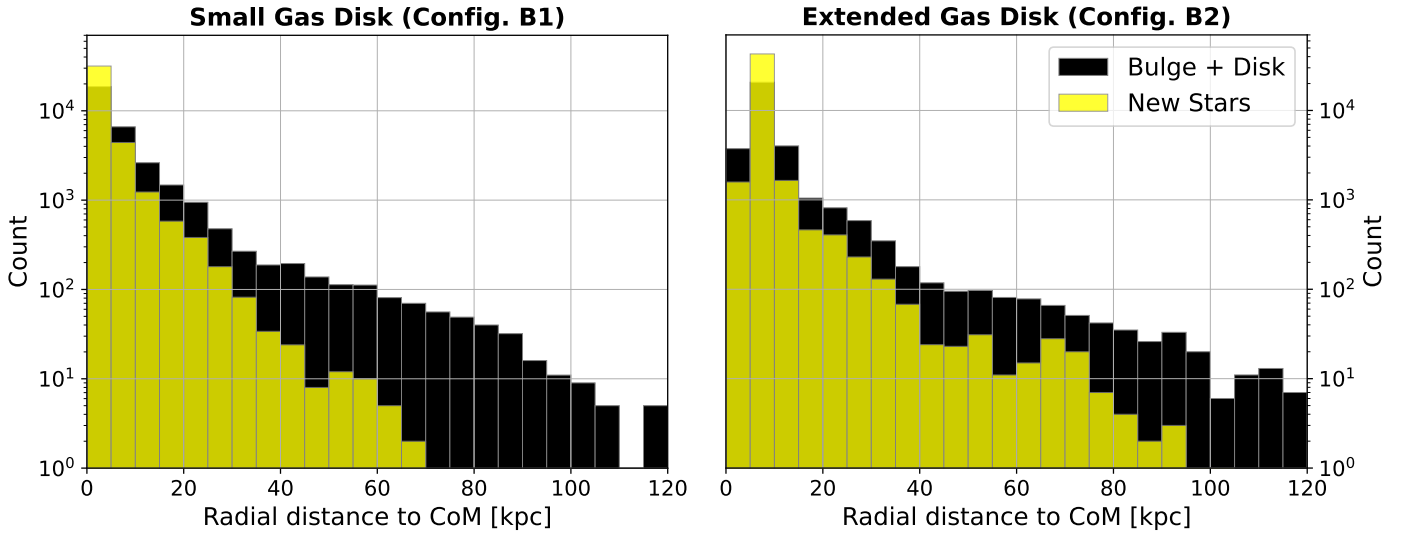
Figure 2.7: Stellar distribution with respect to center of mass (CoM) at $t \sim 850$ Myr.

case with further extended gas mass reservoirs. As already discussed above in Section 2.3, such circumstances supply more advantageous conditions for a tidal dwarf galaxy to become dynamically decoupled from its progenitor as soon as environmental tears are included.

2.5   Extended Merger Catalog

I conclude this chapter of isolated merger studies by providing a compilation of 70 different setups of 2:1 major mergers, where the larger progenitor has a Milky-Way like total mass ($\sim 10^{12} M_\odot$). In each simulation I varied the galaxy properties, as well as their relative impact angle. This collection can be divided in two dynamically different categories: one half of these simulations includes plane-parallel disks, while the other 35 setups initialize perpendicular galactic disks (equivalent to configuration B and A in Figure 2.2, respectively). Since the former case was proven to grant more beneficial circumstances for subsequent dwarf galaxy formation due to the ejection of two equally dominant tidal tails (Section 2.3), I include this catalog here, while the rest is attached in the appendix in Figures A2a to A2d.

Figure 2.8a displays the initial conditions, with their evolution for three different times shown in the subsequent Figures 2.8b to 2.8d. In each row, I vary the impact angle between $0°$ and $90°$, while the initial separation between the galactic centers remains constant at 120 kpc. The first column initializes a prograde, gas-poor merger ($f_{\mathrm{gas}} = 0.2$), with normal-sized bulges ($a_{\mathrm{b}} = 0.2 l_*$, cf. Section 2.1) and similar extents for stars and gas in the disks ($l_{\mathrm{gas}} = l_*$). In each different column, I modify one of those attributes while leaving the rest fixed. Column II includes gas-rich galaxies ($f_{\mathrm{gas}} = 0.2$), column III displays large bulges ($a_{\mathrm{b}} = l_*$) and column IV implements large gas disks ($l_{\mathrm{gas}} = 2l_*$). Finally, column V reveals the development of a retrograde merger, while all galaxy properties compared to column I remain the same.
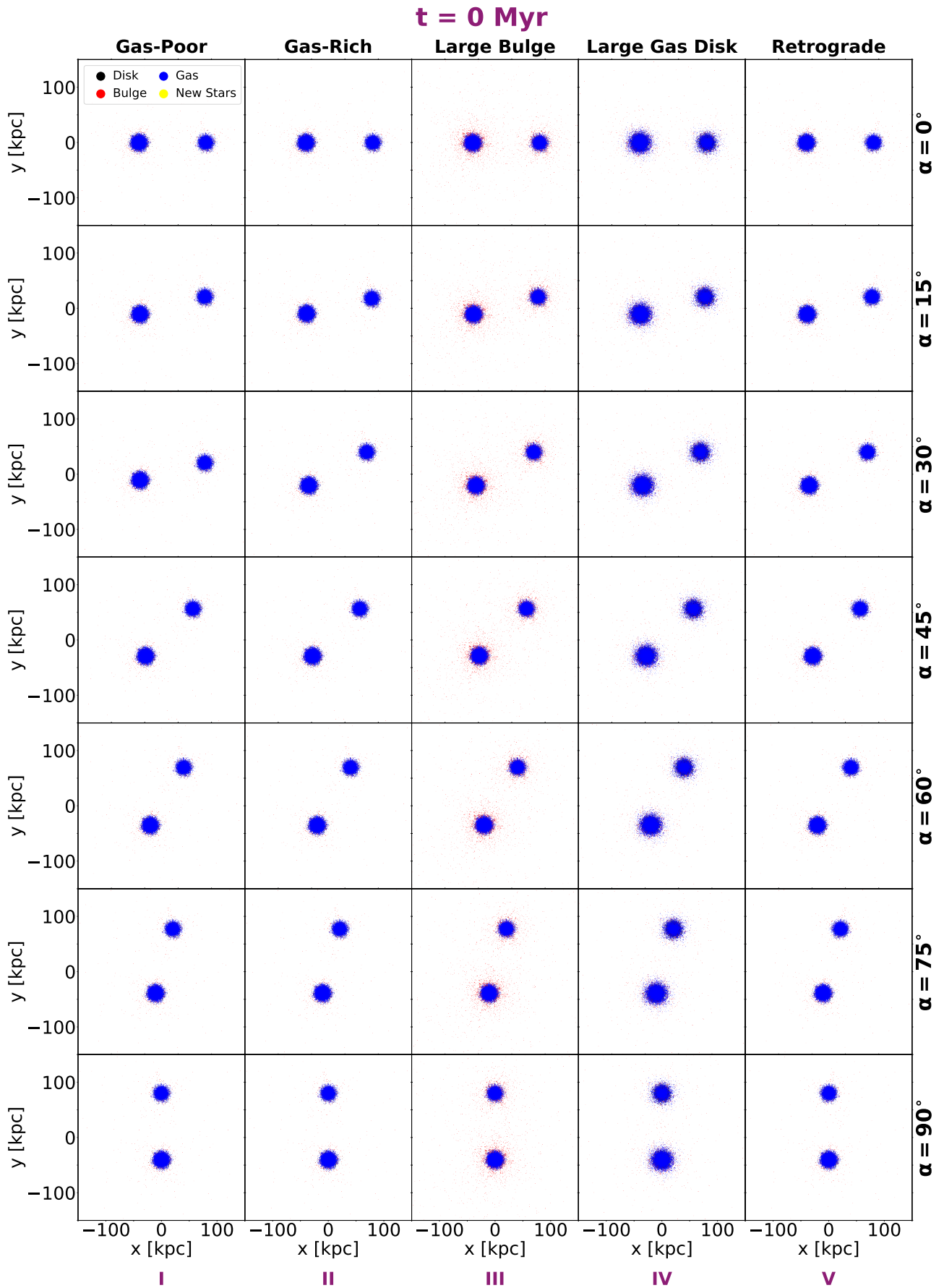
Figure 2.8: Variance of galaxy properties and impact angle in a 2:1 merger with plan-parallel disks.

(a) Initial conditions for merger catalog.

Figure 2.8: Variance of galaxy properties and impact angle in a 2:1 merger with plan-parallel disks.

(b) Time evolution of initial conditions in Figure 2.8a.

Figure 2.8: Variance of galaxy properties and impact angle in a 2:1 merger with plan-parallel disks.

(c) Time evolution of initial conditions in Figure 2.8a.
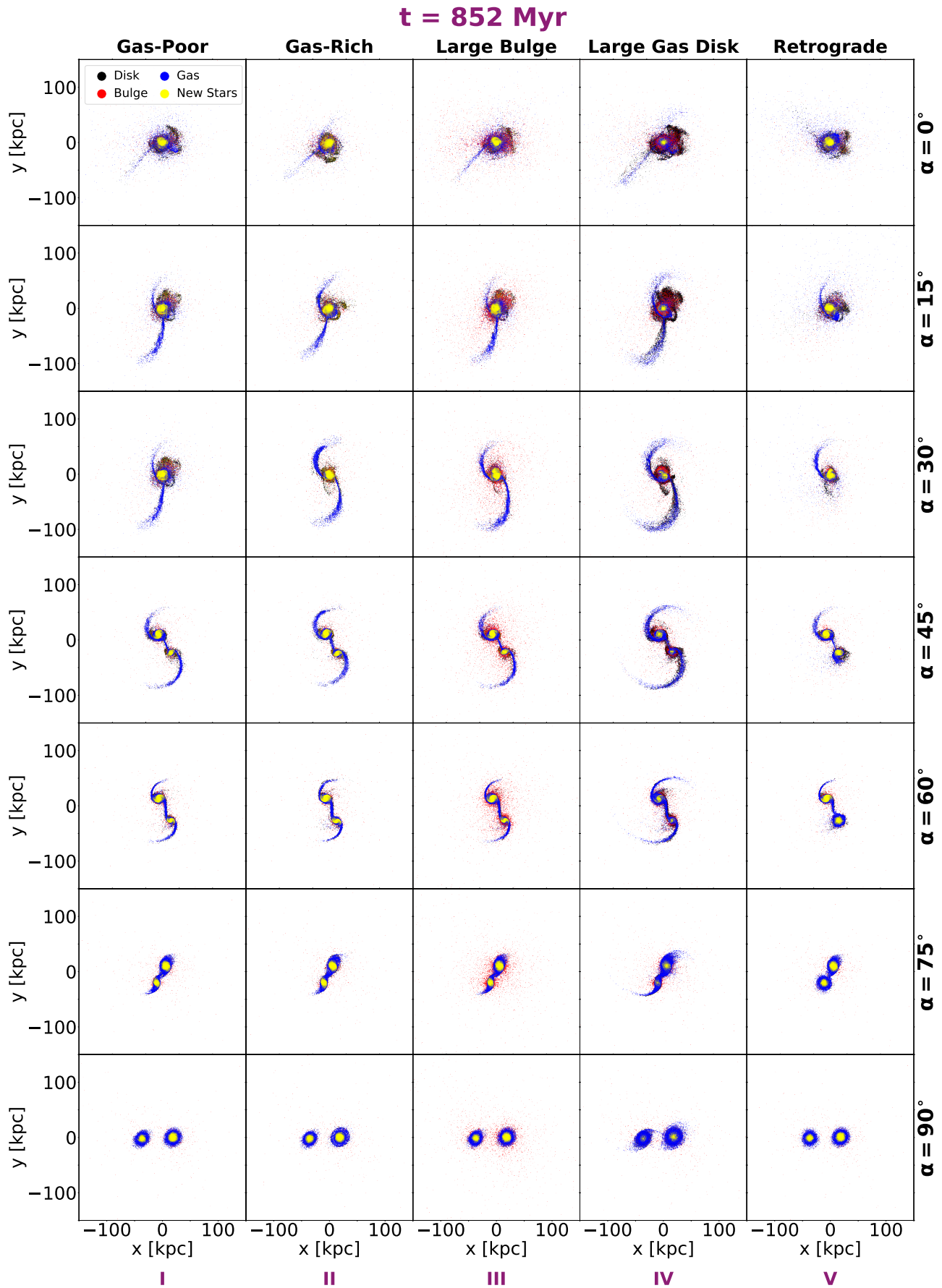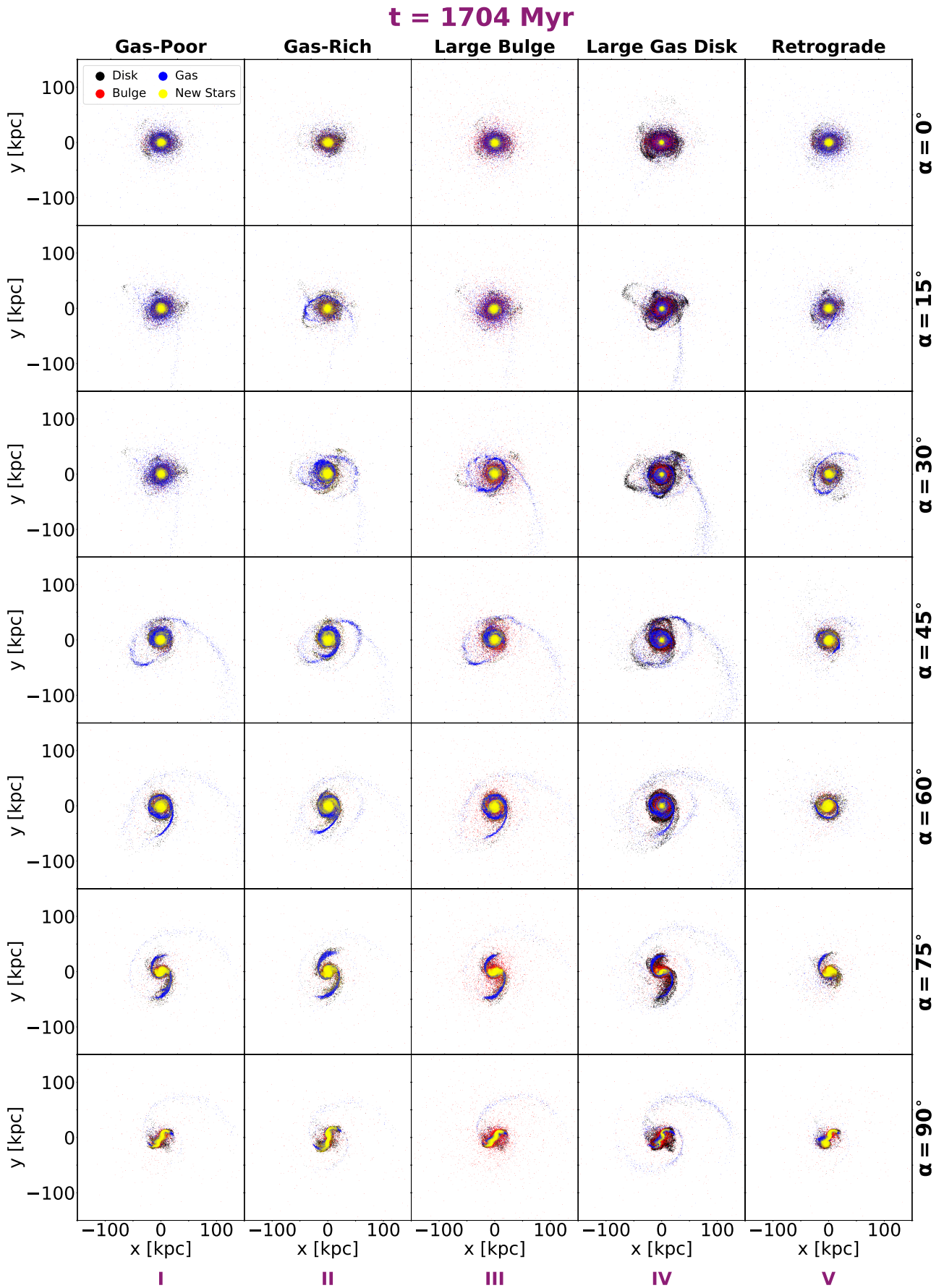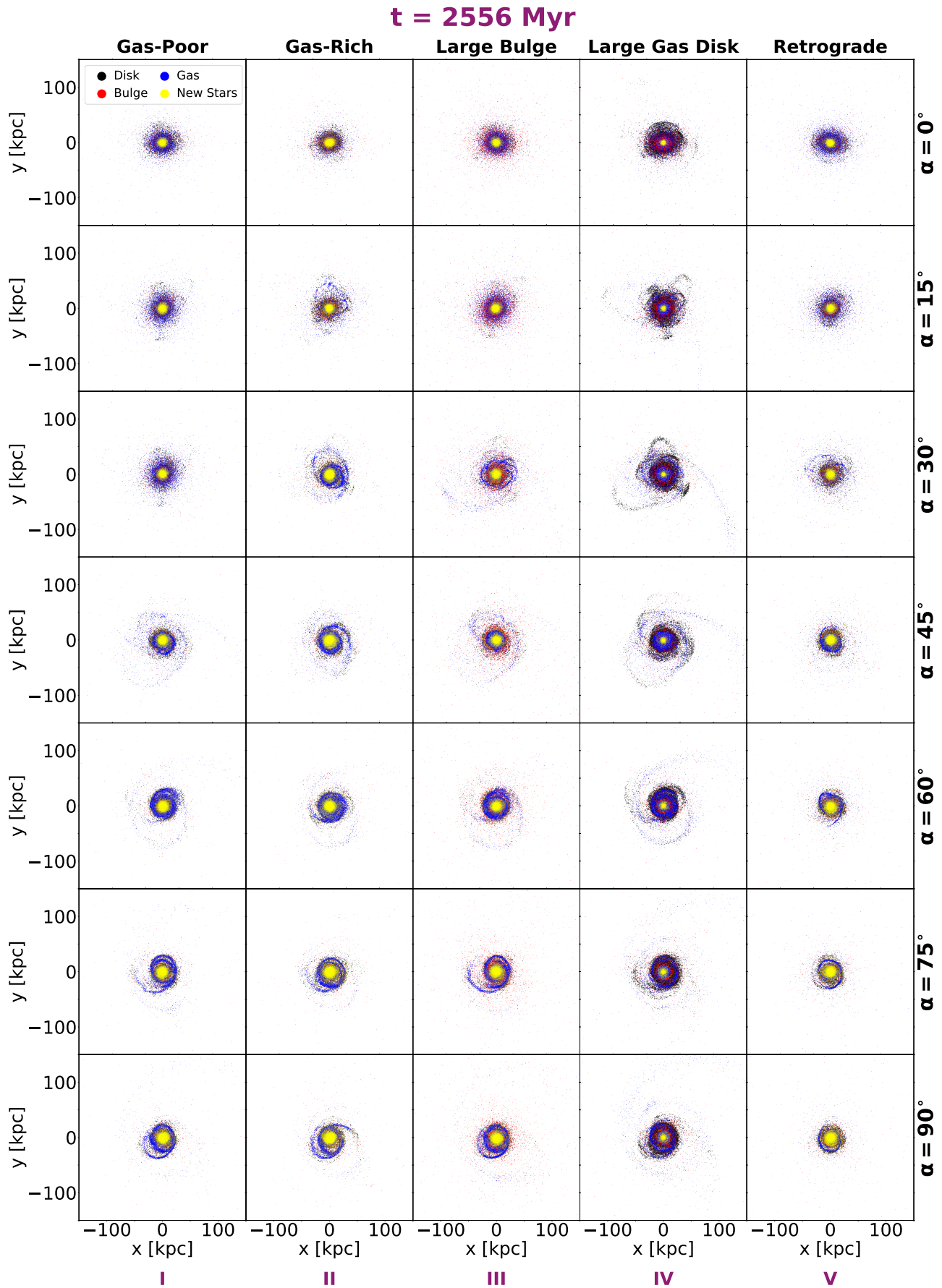
Figure 2.8: Variance of galaxy properties and impact angle in a 2:1 merger with plan-parallel disks.

(d) Time evolution of initial conditions in Figure 2.8a.

Introducing the Cluster: Preliminary Tests

Before stepping into the realm of full scale galaxy merger simulations in clusters, I first needed to set up such an environment. Subsequently followed the nerve-racking tests whether there actually is any qualitative impact on the evolution of a merger at all. It turns out, there definitely is! Hence this chapter is describing the transition phase between my initial isolated merger study and the final analysis of the cluster impact. In Section 3.1, I explain the implementation of a cluster, while its numerical stability is ensured in Section 3.2. Thereafter, Section 3.3 is serving as proof of concept that elevated star formation activity and stripping of tidal features induced by the cluster is indeed occurring.

3.1   General Setup of a Cluster

To create initial conditions for the cluster, I used the method described by Donnert (2014). In this model, the cluster consists of two spherically symmetric distributed components, namely a dark matter halo and hot gas atmosphere, i.e. the intracluster medium (ICM). There is no need to include a stellar component to the cluster apart from the analysed galaxy merger since the stellar component typically composes only a small fraction of the total cluster mass and because galaxy mergers inside the virialized region of a galaxy cluster are rare due to the high velocity dispersion of the cluster members.

Following the same arguments as in the setup of the dark matter component of a galaxy, the cluster halo is modelled by a Hernquist distribution (cf. Equation 2.2), which closely follows an NFW-profile in the inner regions, but declines steeper at larger radii and thus results in a finite total mass. The ICM, on the other hand, is modeled by the β-model (Cavaliere & Fusco-Femiano, 1978), which is motivated by observations (Croston et al., 2008). Thus we have

$$\rho_{\text{ICM}}(r) = \rho_0 \left(1 + \frac{r^2}{r_c^2}\right)^{-3\beta/2}, \tag{3.1}$$

where ρ_0 is the central gas density and r_c the core radius of the gas distribution. Following the cluster simulations by Mastropietro & Burkert (2008), the exponent parameter is set to

$\beta = 2/3$. The baryon fraction inside the virial radius R_{200} of the cluster is $f_{\text{bar}} = 0.14$.

Although the cluster in which the observed comparison merger NGC 5291 is taking place has a mass about twice as high (Oh et al., 2018), I chose the virial mass of the simulated cluster to be $M_{200} = 10^{14} M_{\odot}$ throughout this work. I decided on this value as a compromise to stay in the range of typical cluster masses, while keeping the computation time at bay, since simulating the galaxy cluster is quite expensive due to the large number of SPH particles.

3.2   Cluster Stability Test

Before I could start examining environmental influences on the evolution of a galaxy merger, I needed to ascertain that the cluster model is behaving well and stays stable for a significant period of time. For this purpose, I initialized a cluster with a virial mass of $M_{200} = 10^{14} M_{\odot}$ and probed its density evolution over ~1 Gyr. Such a test does not require profuse resolution, which is why I chose a coarse sampling, resulting in a particle mass of $m_{\text{dm}} = 3.6 \times 10^{9} \, M_{\odot}$ and $m_{\text{ICM}} = 0.7 \times 10^{9} \, M_{\odot}$ for dark matter and gas, respectively. The left-hand side of Figure 3.1 shows the mass density for both components, which was estimated by counting the particles present in logarithmically equidistant spherical shells and weighting them with their respective mass. To illustrate the appearance of the cluster, its spatial distribution is drawn with the same color coding as in the histogram beside, namely black for the dark matter halo and cyan for the hot gas atmosphere. The radial distance R to the center of mass is plotted in terms of the object's virial radius $R_{200} = 957$ kpc, which follows from the applied virial mass by assuming a Hubble parameter of $h = 0.7$. The line opacity increases with each progressive snapshot.

Apart from the innermost regions, the cluster is absolutely stable up to its outskirts at $3R_{200}$. The small volume of the spherical shells close to the centre cause the density estimate to be overly sensitive for the number of enclosed particles, which undergo constant in- and outflow due to the endeavored equilibrium. These fluctuations are therefore no reason for concern, particularly because the central regions are not relevant for my experiment anyway. Galaxy mergers can only take place if their relative velocities are low enough in the first place – this prerequisite is typically not met inside the virialized region of a cluster, where its dispersion velocity is already too high. Besides, a proper model of the innermost cluster areas would require a central massive galaxy anyway. Hence the stability of the environment is assured at the relevant regions around its virial radius and in the outskirts, allowing to proceed towards galaxy merger simulations in a cluster.
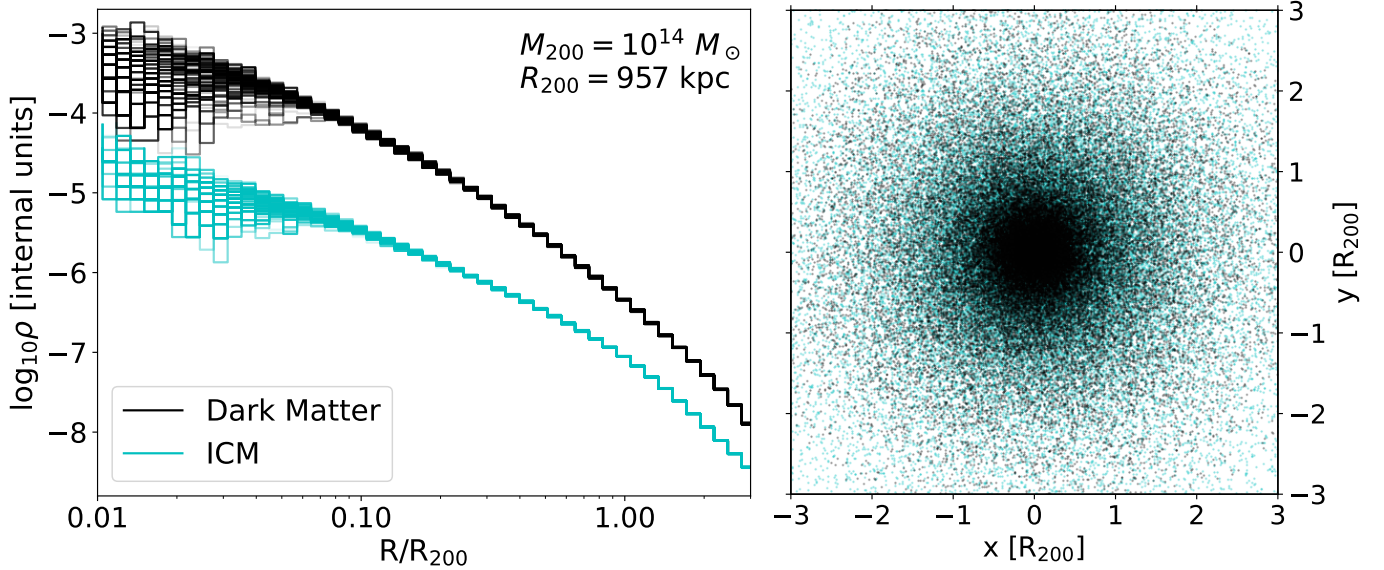
Figure 3.1: *Left:* Density evolution in a cluster over a period of ~1 Gyr. The line opacity increases with proceeding time. *Right:* Particle distribution in the initialized cluster.

3.3 Changes in Merger Evolution Through the Cluster

Arranging a merger inside a cluster required two additional fundamental choices for the initial conditions, namely the starting position and velocity of both galaxies with respect to the cluster. As explained in Section 3.2, their initial distance to the cluster center should not be chosen to low, since in reality the dispersion velocities between cluster members inside virialized regions are too high to permit collisions. However, mergers certainly do happen while the members are still flowing towards the cluster inside filaments of the Large Scale Structure. The relative velocity between objects in such regions is comparable to their virial value, as already encoded in the isolated merger initial conditions (cf. Section 2.1). With these considerations in mind, the galaxy merger was decided to be initialized at a radial distance of $2R_{200}$ with a relative velocity of V_{200} for all participating particles with respect to the cluster center. R_{200} and V_{200} refer to the virial radius and velocity of the cluster, respectively. The galaxy interaction itself was initialized as a prograde merger with a mass ratio of 2:1 and plane-parallel, gas-rich disks ($f_{gas} = 0.8$). The large impact angle and initial separation between the central black holes of $\alpha = 36°$ and $d_{sep} = 140$ kpc, respectively, was chosen to create advantageous conditions for the formation of pronounced tidal tails (cf. Chapter 2). To maximize the star formation resolution while also keeping the computational cost at bay, I relied on my results from Section 2.3, choosing $m_{bar} = 6.5 \times 10^5\ M_\odot$ and $m_{dm} = 3.2 \times 10^6\ M_\odot$ for the baryonic and dark matter component, respectively. Since I am particularly interested in the interaction between the hot ICM and the cold gas carried by the galaxies, I implemented the same particle resolution for both of these components, because otherwise my results could be contaminated by numerical artifacts. Due to the enormous amount of SPH particles contributed by the cluster, such a choice led to skyrocketing numerical costs. Nevertheless it is worthwhile, as we will see soon.
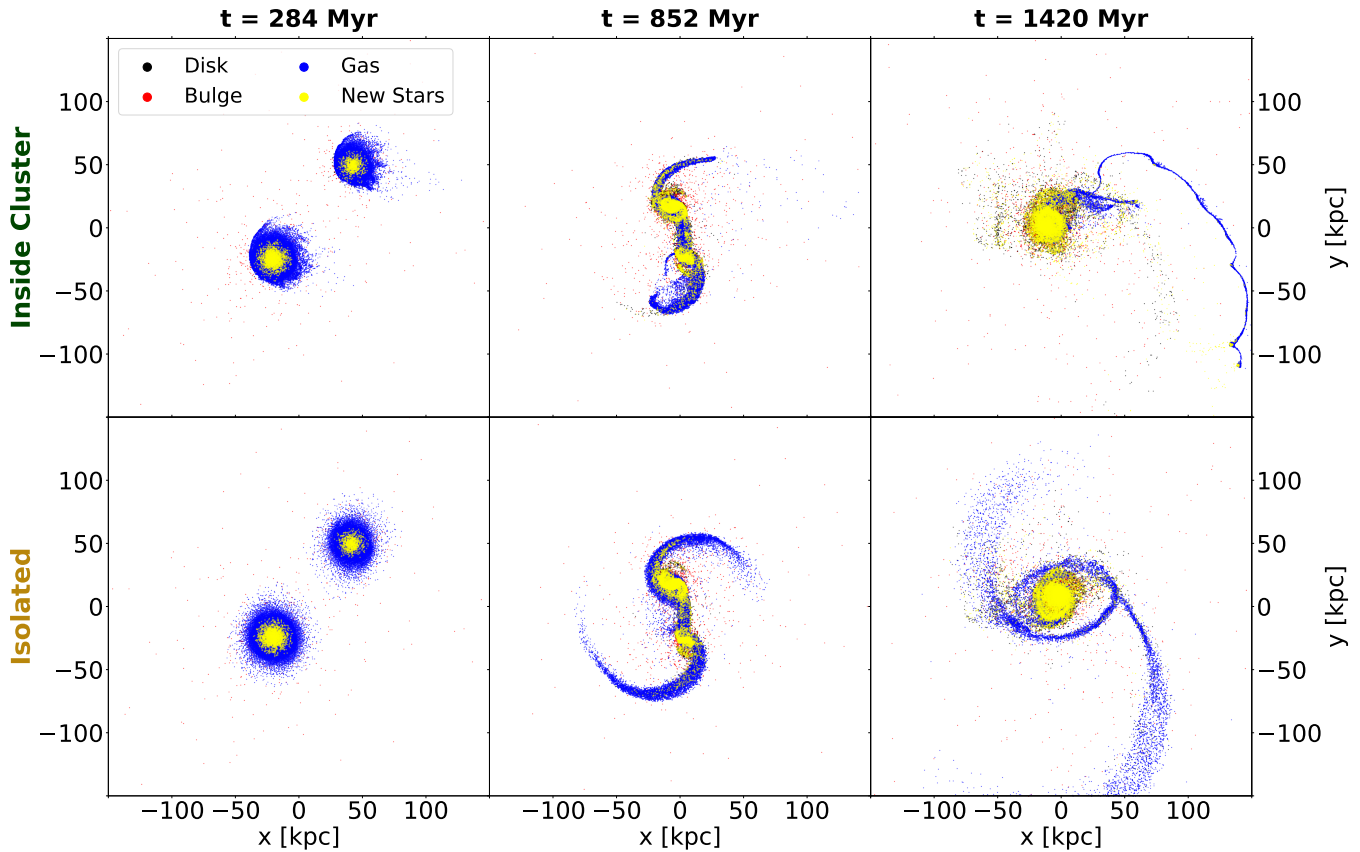
Figure 3.2: Morphology evolution of a galaxy merger in a cluster environment. The isolated merger is shown in the row below for comparison.

Figure 3.2 illustrates the spectacular differences in the merger morphology caused by interactions with the environment (top row) compared to the isolated test case (bottom row). The galaxies are falling radially into the cluster and therefore experience ram pressure in that direction, which in this case is parallel to the x-axis. I do not plot the intracluster gas here, to highlight the arising differences in the distribution of tidal gas. The impact of the strong headwind can be seen in the first column before the merger even has happened as "fraying" of the galactic gas disk. Later on, ram pressure continues to rip off the low-density tips of the gaseous tidal tails (middle column). At this point we can already notice another crucial environmental influence: this continuous push by the ICM causes the tidal tails to become thinner and more compact. The upper feature disperses entirely, since its rotation causes the local gas to experience elevated ram pressure due to the increased relative velocity. The lower arm, however, has a decreased relative velocity and therefore experiences lower ram pressure than the rest. Hence it manages to harbour its gas, while also undergoing substantial compression due to open exposure to the headwind. This process eventually triggers the genesis of several star forming pockets inside that tidal tail, which are then collectively stripped together with the whole tidal complex (right column).

To demonstrate the drastic behavioural shifts in terms of star formation activity, I trace at which radial distance with respect to the merger center new stars are forming in the tidal tails (cf. Section 2.3) and count the number of these particles per radial bin in Figure 3.3. The
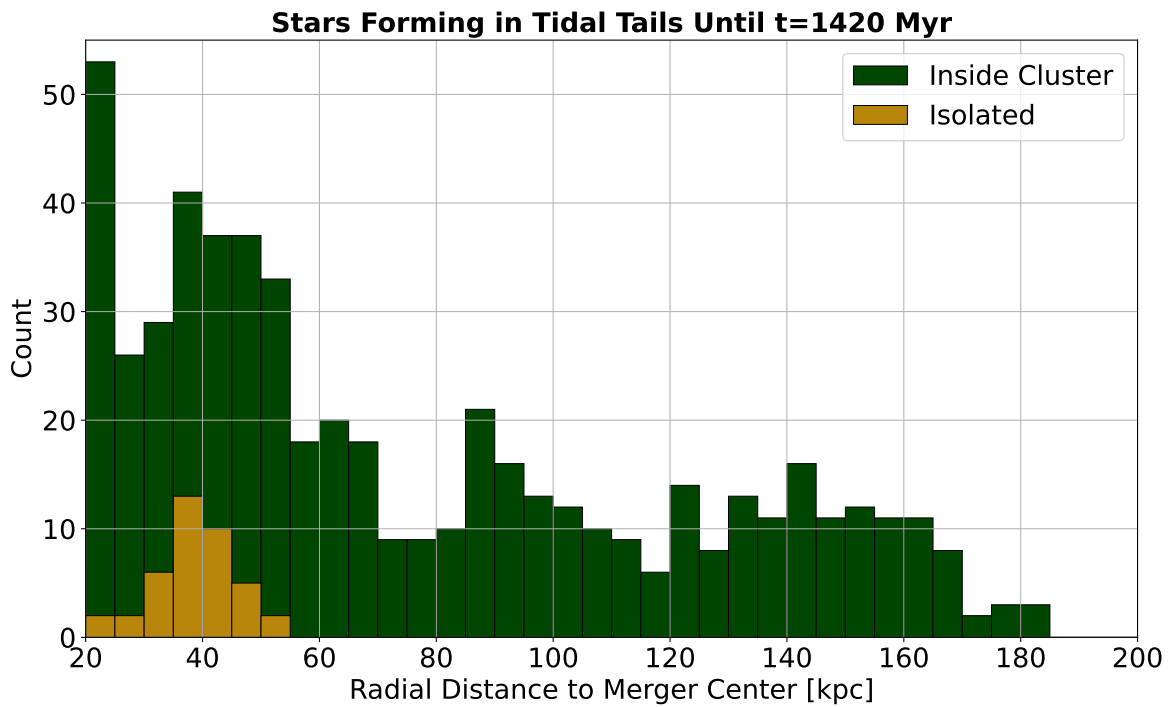
Figure 3.3: Star formation in tidal tails against radial distance to the progenitors's center of mass for galaxy mergers with included (darkgreen) and excluded (lightbrown) environment.

count is cumulative up until the moment of the third column in Figure 3.2. I plot the simulation with an included environment in darkgreen, while the isolated case is shown in lightbrown. The elevated density inside the tidal tails exposed to the ICM leads to significantly higher star formation rates compared to the isolated merger. On top of that, we can see how the environment is enabling star formation at much farther distances to the merging progenitors. Such newly formed tidal dwarf galaxies are therefore only loosely bound to their parents' potential well, enabling them to ultimately escape into the cluster. These results are of major importance for this thesis, since in principle my project could be boiled down to one question: Can environmental interactions pose as an evolutionary channel towards low-mass objects through stripping of tidal dwarfs galaxies? Now finally, Figures 3.2 and 3.3 prove – yes, it is in fact possible.

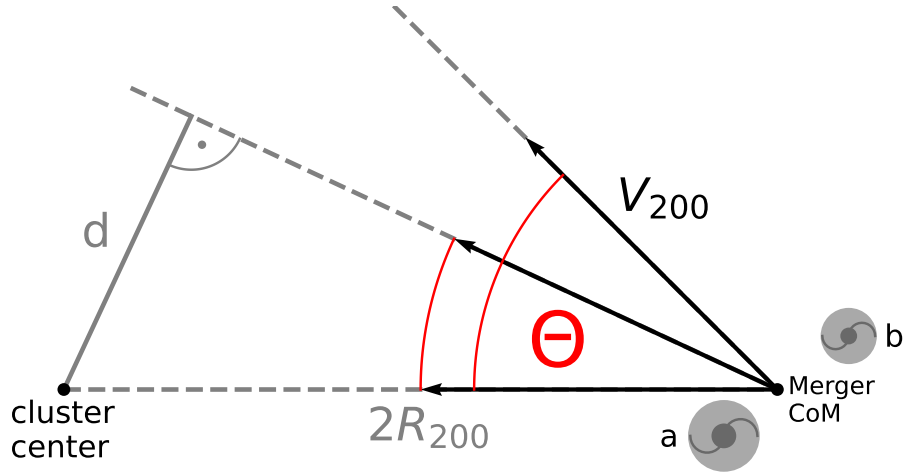# Stripped Tidal Dwarf Galaxies: a Quantitative Analysis

At this point, the groundwork is finally set for the real experiment. I have established in the chapter before, that cluster environments causes significant changes in the behaviour of the galaxy merger. In particular, I found much further extended tidal features, elevated star formation activity and stripping of newborn tidal dwarf galaxies from their progenitor. Such circumstances inspire several exciting questions: What kinds of new objects are forming? Are these stripped tidal dwarfs able to persist under the hostile cluster conditions? What is their long-term evolution? Therefore, I performed a simulation campaign in high resolution of galaxy mergers in a cluster environments. I summarize the parameters and qualitative results of the sample in Section 4.1. The results are reviewed in the subsequent Sections, where I analyse and compare the simulation outcomes and give answers to the questions above.

4.1   Configuration of the Simulation Sample

Following the arguments presented in Section 3.3, I choose the starting distance of the galaxy merger to be at $2R_{200} \approx 1.9$ Mpc, while their initial velocity with respect to the cluster is taken to be $V_{200} \approx 670$ km/s. R_{200} and V_{200} refer to the virial radius and velocity of the cluster, respectively. The implementation details of the cluster, consisting of a dark matter halo and hot gas atmosphere, can be found in Section 3.1. To investigate the orbital impact on the emerging satellite dwarf population, I vary the impact angle Θ of the merger with respect to the cluster. Specifically, I implement a radial infall, i.e. $\Theta = 0°$, and two elliptical orbits with $\Theta = 25°$ and $\Theta = 45°$, respectively. Meanwhile, the galaxies' orientation towards the cluster centre and the merger configuration remains the same. I implement the same merger as in the initial environmental studies in Chapter 3 – namely a prograde, gas-rich merger with a mass ratio of 2:1 and plane-parallel disks, colliding with a large impact angle. Such an orbit is equivalent to configuration B from the isolated merger studies in Chapter 2, which is why I used this letter in the parameter description in Table 4.1a. The geometrical setup is illustrated in Figure 4.1.

Table 4.1: Main parameters of initialized simulation sample.

(a) Impact values with respect to cluster center.

Config.	Angle Θ [°]	Parameter d [Mpc]
B0	0°	0
B25	25°	0.8
B45	45°	1.3

(b) Virial masses, radii and velocities of objects.

	M_{200} [10^{12} $M_\odot$]	R_{200} [kpc]	V_{200} [km/s]
Cluster	100	957	670
Galaxy a	1.4	229	160
Galaxy b	0.7	181	127

Figure 4.1: Illustration of the implemented simulation sample. The setups vary in their impact angle Θ according to Table 4.1a.

The main parameters of the created cluster and two galaxies are listed in Table 4.1b. I chose the same resolution $m_{\mathrm{bar}} = 6.5 \times 10^5$ $M_\odot$ for all gas particles in the simulation volume, i.e. for those initially associated to the galaxies, as well as for those contained by the cluster. This way, the simulation can properly resolve gas interactions between the cluster and the galaxies, without contaminating the results with numerical artifacts due to different resolutions between the SPH particles. The stellar resolution is the same as for the gas, while the dark matter resolution is $m_{\mathrm{dm}} = 3.2 \times 10^6$ $M_\odot$. The total simulation volume is a cube with boxlength $2 \cdot 3.75 \cdot R_{200,\mathrm{cluster}} = 7.2$ Mpc.

Tidal dwarf galaxies are formed and stripped in all three orbit configurations. On its left hand side, Figure 4.2 shows a snapshot[1] of configuration B45. I rendered gas and young stars in yellow and lightblue, respectively, using the raytracing visualization software Splotch (Dolag et al., 2008). This Figure highlights the significant gas compression occurring in the tidal features, which in turn triggers pockets with elevated star formation activity. This process is induced by the merger impact, as well as by ram pressure through the intracluster gas, with the latter being more dominant at larger distances to the merger centre. This process gives birth to pockets with high star formation, highlighted by circles in Figure 4.2. Although there are tidal dwarfs which eventually fall back into their progenitor (dashed circles), the majority of them is able to escape the local potential and starts to evolve independently (solid

---

[1]The full movie is available on YouTube: `https://youtu.be/EQyEK1qQAhU?si=ut7LaY2GTI5yf4kB`

circles). The right hand side of Figure 4.2 displays the spatial distribution of stripped tidal dwarfs (black dots) formed by a galaxy major merger moving through a cluster ~3 Gyr after the beginning of the simulation (configuration B45). The dashed line traces the trajectory of the galaxy merger, while the blue background indicates the intracluster gas. Curiously, I also find two stripped tidal dwarfs in this simulation configuration, which form a rotationally supported double-system for ~2 Gyr, after which they merge and become a single dwarf galaxy (orange circles in Figure 4.2). In the radial infall scenario B0, all dwarf structures are quickly destroyed after about 1-2 Gyr by tidal forces upon passage through the cluster centre. In the elliptical orbits B25 and B45, however, the dwarf galaxies manage to survive much longer for up to ~4 Gyr, while spiraling inwards towards the cluster centre.
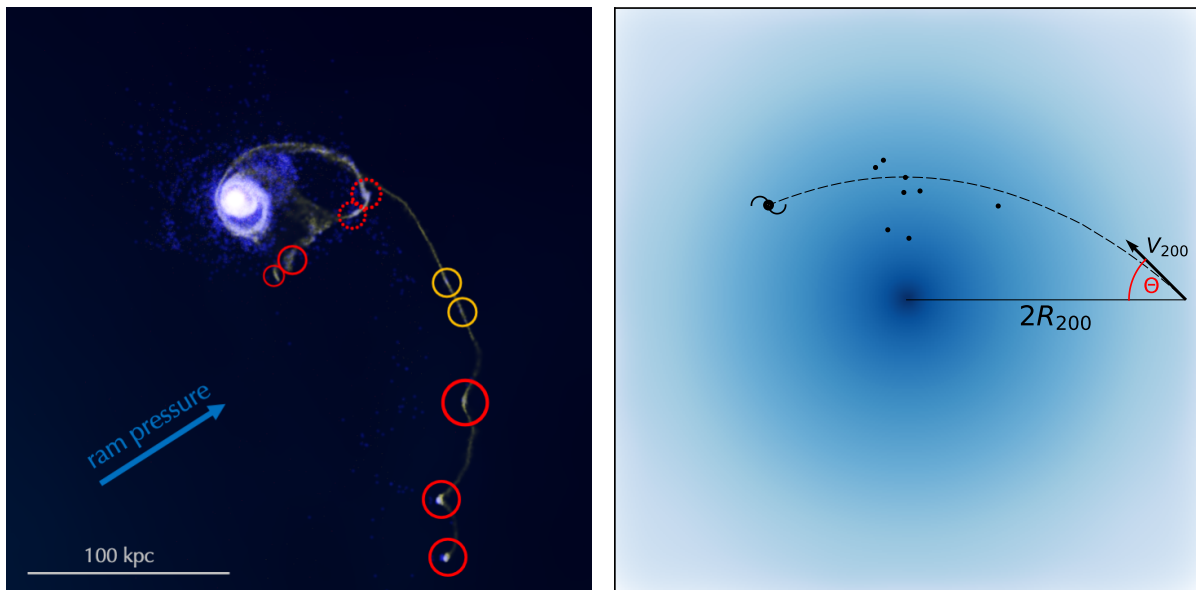

Figure 4.2: *Left:* Simulated galaxy merger on an elliptical orbit (B45) in a cluster. *Right:* Tracks of stripped tidal dwarf galaxies inside a cluster.

4.2 Evolution in Phase Space

By visually inspecting the simulation in real and phase space, I identify the position and extent of dwarf galaxies, which are disassociated from the galaxy merger remnant. I start to analyse the dwarf galaxies ~300 Myr after the first stellar clumps started forming in the tidal tail of the merger, because they first needed to get stripped before one could identify the structures as isolated dwarfs. Figure 4.3 displays two examples of dwarf galaxies forming on a radial (upper panels) and elliptical (lower panels) orbit in the cluster. The top and bottom row of each case show the distribution in real and phase space, respectively, while the columns are snapshots at three different times. The stellar content of the dwarf, identified at the moment of the middle panel, is traced in red. The gas density is visualized in blue, while stars are plotted in yellow or grey in real and phase space, respectively. For estimating the clustercentric distance in the phase space plots, I compared the relative position of a particle to the center of mass of the cluster. The population around $r = 0$ visible in these figures

corresponds to stars forming at the cluster center, since by construction the cluster initially does not have a BCG, which is why the gas starts to cool and ignite star formation there.

It is clearly visible, how the stellar content of the traced dwarf is seeded in the high density regions of the tidal tail in both simulations. The radial scenario causes a rapid infall, resulting in a swift stripping event of tidal features due to increased ram pressure. A merger on an elliptical orbit, on the other hand, is able to harbour its tails for a longer period. Accordingly, stellar structures have more time to develop in that case. Their traces are already visible in the earliest panel of $\Theta = 45°$ as a characteristic edges in the tidal tail. They are a consequence of ram pressure, which is exercising a headwind on the gas component from the left hand side, but inherently is not acting on the embedded stellar population. Yet, the gravitational potential of these pockets is dominated by the mass of the gas. The new stellar population, forming out of collapsed gas, is naturally located in the regional potential wells. As a result, stars are also being stripped as soon as gas clumps are being ripped from the progenitor by the environment.

After detaching from their parents, the tidal children begin to develop independently. This becomes apparent by comparing the position in phase space between the dwarf and the merger remnant (the largest symmetric structure), indicating that the tidal object is becoming dynamically decoupled. Constantly under pressure because of the ICM, the dwarf galaxies are exhibiting high star formation rates. Although continuously converting their gas content into stars, they still maintain their gas-dominated composition. At the moment of the middle panel, the dwarfs have total masses of $M_{\text{tot, B0}} = 8 \times 10^8 \ M_\odot$ and $M_{\text{tot, B45}} = 7 \times 10^8 \ M_\odot$ with gas mass fractions of 10% and 24% for the radial an elliptical merger orbit, respectively. Meanwhile, they are completely devoid of dark matter, as they originated from the tidal sites outside the progenitor's potential well center, where less dark matter particles were present. The dwarfs do not keep their full stellar body during their evolution though. We can see in the uppermost middle panel, that the dwarf galaxy is developing a *leading* tail of stars. This curiosity will be addressed in further detail in Section 4.7.

In case of the radial infall scenario, the system naturally evolves on a shorter timescales, since the merger reaches high density regions inside the cluster much faster. Hence I also have chosen a shorter timestep between consecutive panels for B0 to be half as long (~0.5 Gyr), than for B45 (~1 Gyr), in order to properly visualize the environmental impact on the dwarf galaxy. The evolution in the bottom panel ($\Theta = 45°$) is mainly dominated by interactions with the ICM, hence the dwarf continues to move on an autonomous orbit. The object on a radial orbit, however, leads a more turbulent lifestyle. Having almost none angular momentum with respect to the cluster, the progenitor, as well as its tidal dwarf galaxies are destined to fall into this massive central potential well, visible as the dark blue spot in the latest time panel. As a result, all structures are "stretched" out both in real and phase space by the tidal field, which even rips the traced dwarf apart into two separate remains.
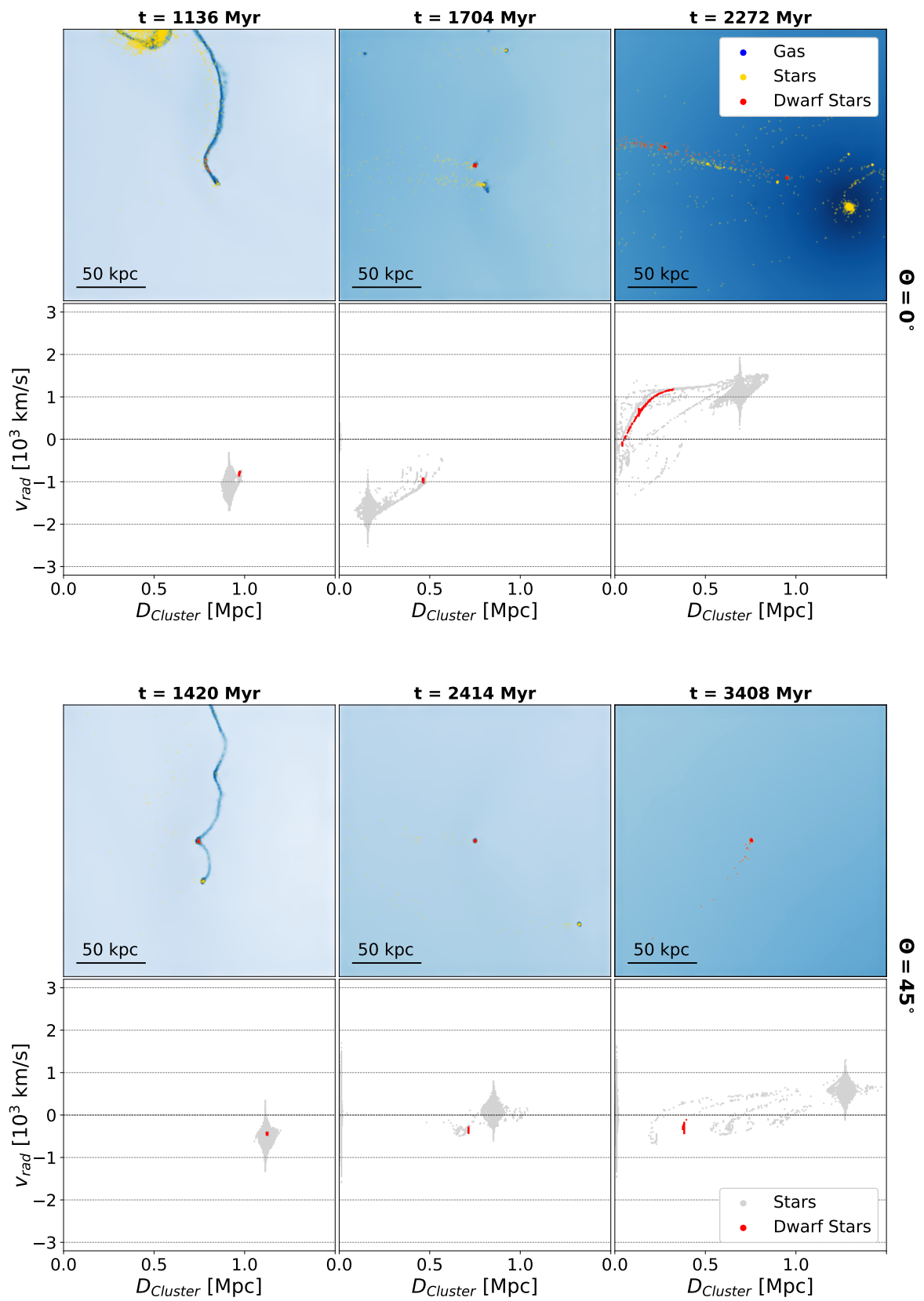
Figure 4.3: Real space vs. phase space distribution of a dwarf forming on merger orbits B0 (top) and B45 (bottom) for three different moments in its evolution. The timestamp at the top specifies the period elapsed since the beginning of the simulation.

4.3   Mock Images

For illustration purposes, I created mock observations of a few stripped tidal dwarfs in Figure 4.4, using the software by Martin et al. (2022). The first two on the left show dwarfs from the radial infall scenario (B0), while the other two on the right display objects forming on an elliptical orbit (B45). Since most of the dwarfs form at similar times in the same environment – namely, the tidal tail of the merger – we can observe alignment in some cases, which creates the effect of "pearls on a string". The rightmost panel, on the other hand, shows a rotationally supported double-system of dwarf galaxies, which was formed from two separate tidal dwarfs in the merger (cf. orange circles in Figure 4.2). I identify it as one dwarf, since it is a gravitationally bound system and – depending on the resolution of the telescope – it could be classified as one object in observations as well.
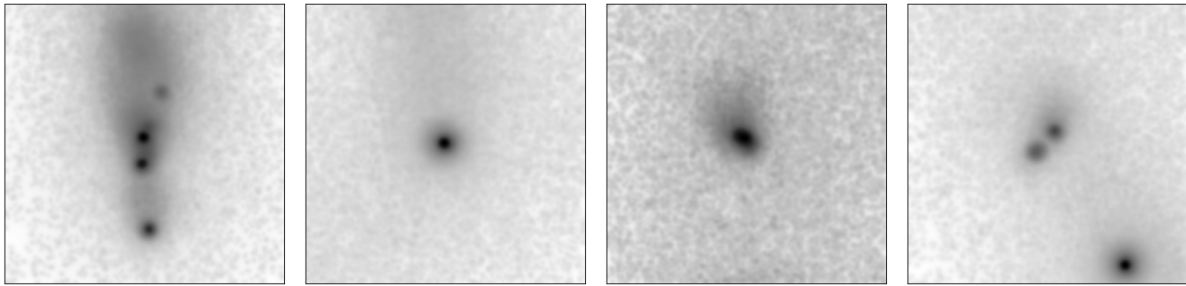

Figure 4.4: Mock observations of simulated tidal dwarfs.

4.4   Dwarf Tracks Inside the Cluster

Dwarf galaxies forming in a radial infall scenario quickly reach the cluster centre due to lack of initial angular momentum, whereas objects forming on elliptical merger orbits naturally survive for a longer period of time. As visible in Figure 4.5, most of them spiral inwards, while continuously loosing momentum due to friction between the dominating gas component of the galaxies and the intracluster gas. The grey background indicates the cluster gas density, while the different shades of orange (B25) and blue (B45) represent progressively advancing time in the dwarf tracing. Curiously, there is an outlier in terms of dynamical behaviour in B45, which quickly adapts a radial orbit and moves much slower than the rest. This is the smallest dwarf galaxy in that sample, which barely surpasses the resolution threshold, having a final gas and stellar mass of $M_{\mathrm{gas}} = 4 \times 10^7 \, M_\odot$ and $M_* = 10^6 M_\odot$, respectively. The comparably small mass causes the dwarf to loose its angular momentum due to friction on much shorter timescales, while ram pressure is also simultaneously slowing down the radial infall of the gaseous dwarf galaxy. A massive object, on the other hand, is less impacted by environment, such as as the dwarf in B25 tracing a hook-like orbit, resulting in the largest final clustercentric distance within the sample.
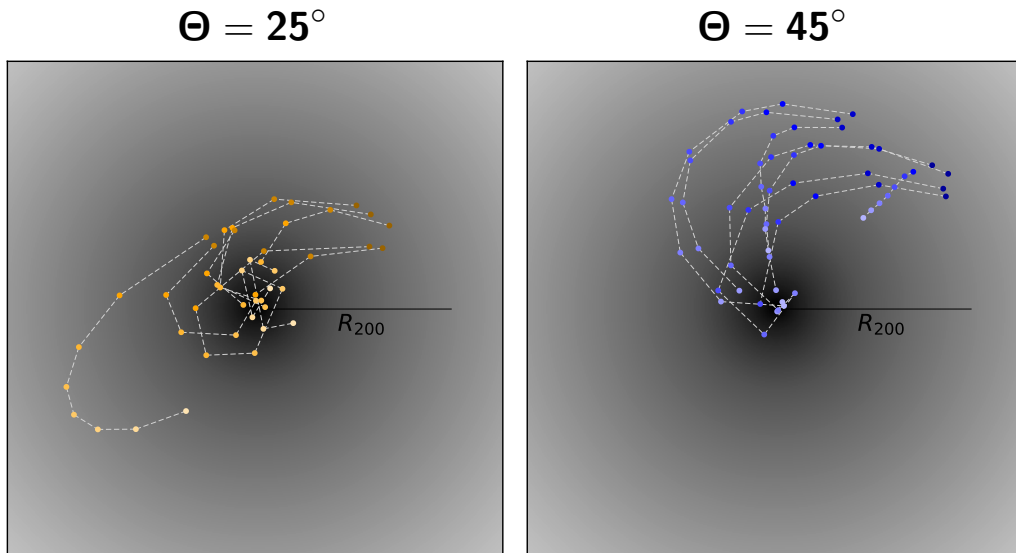
Figure 4.5: Tracks of stripped tidal dwarf galaxies in a cluster over a time period of ~4 Gyr. Consecutively lighter shades indicate progressively later times, with a time step of ~0.5 Gyr between evaluations.

4.5 Categorizing the Zoo

To understand what kind of objects are forming, I compare the simulated dwarfs in Figure 4.6 with a a broad range of types observed in the nearby Universe. This figure shows how different types of objects populate distinct regions in the stellar size vs. luminosity plane. The vast majority of observed objects, spanning from giant ellipticals to stellar clusters, was compiled by Brodie et al. (2011). I also include data of ultra-diffuse galaxies (UDGs) for comparison, indicated by triangles. UDGs in the Coma cluster by van Dokkum et al. (2015) are plotted in grey, while the lightblue and pink triangles represent gas-rich field UDGs by Jones et al. (2023) and the two UDGs NGC1052-DF4 and DF2 by Cohen et al. (2018), respectively. The latter case has been speculated to have formed through a high-velocity collision of gas-rich galaxies (Lee et al., 2021; van Dokkum et al., 2022). In the upper panel, I plot the time evolution of stripped tidal dwarf galaxies from all three simulations (B0, B25 and B45) in purple for three different times, being ~2 Gyr apart and distinguished by consecutively lighter shades. The bottom panel is the exact same figure, but distinguished in the dwarfs' respective merger orbit. Their luminosity of the simulated dwarf galaxies was estimated by applying age dependant mass-to-light ratios provided by Sextl et al. (2023) for each stellar particle. Comparing their position to the observed objects, we see that the tidal dwarf galaxies mostly populate a gap between compact and dwarf ellipticals (cE, dE) and dwarf spheroidals (dSph). Curiously, there is also a small overlap between observed UDGs and our simulated dwarf galaxies at the large size end. This overlap is observed at earlier stages during the first ~2 Gyr of their evolution, since the dwarfs tend to decrease in stellar size during their infall in the cluster (cf. Section 4.7). In summary, these results are suggesting that environmental stripping of tidal dwarf galaxies could be an evolutionary channel towards a variety of low-luminosity objects, such also for gas-rich, dark matter deficient UDGs.
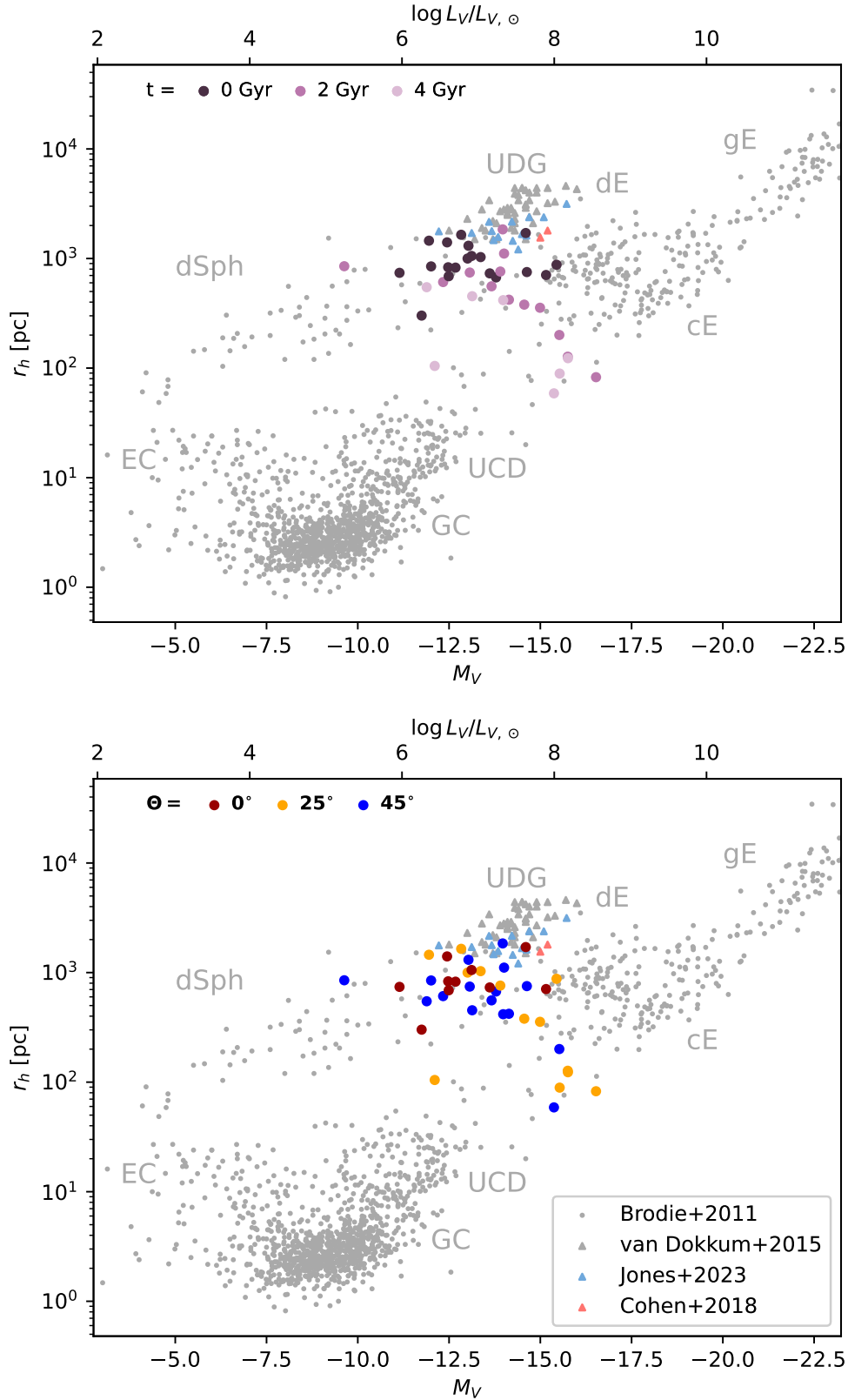
Figure 4.6: Relationships between half-light radii and visual band luminosities for various types of objects observed in the local Universe, as well as for the simulated tidal dwarf galaxies. Grey circles show stellar systems in our local environment including giant, compact & dwarf ellipticals (gE, cE & dE), dwarf spheroidals (dSph), ultra-compact dwarfs (UCD) and globular & extended clusters (GC & EC) compiled by Brodie et al. (2011). Grey triangles represent ultra-diffuse galaxies (UDG) observed in the Coma cluster by van Dokkum et al. (2015). Colored triangles show special cases of UDG, namely gas-rich field UDG in lightblue by Jones et al. (2023) and NGC1052-DF2 and DF4 in pink by Cohen et al. (2018).

4.6   Gas Mass Loss

Since they originate from the tidal gas tail of the galaxy merger, the stripped tidal dwarfs exhibit high gas mass fractions and are generally dark matter deficient, as becomes apparent by Figure 4.7, which shows their gas vs. total mass. The three tested orbit scenarios of a galaxy merger falling into a cluster with an infall angle of $\Theta = 0°, 25°$ and $45°$ are represented by red, orange and blue markers, respectively. Consecutively lighter shades represent progressing time between $t = 0 - 4$ Gyr with time steps of ~0.5 Gyr. Young dwarfs are entirely gas dominated, but increase their stellar mass component over time due to ongoing star formation, boosted by ram pressure. The slight decrease in total mass points towards environmental gas stripping as well. Interestingly, the dwarfs with the largest gas mass reservoir also experience the highest relative gas mass loss.
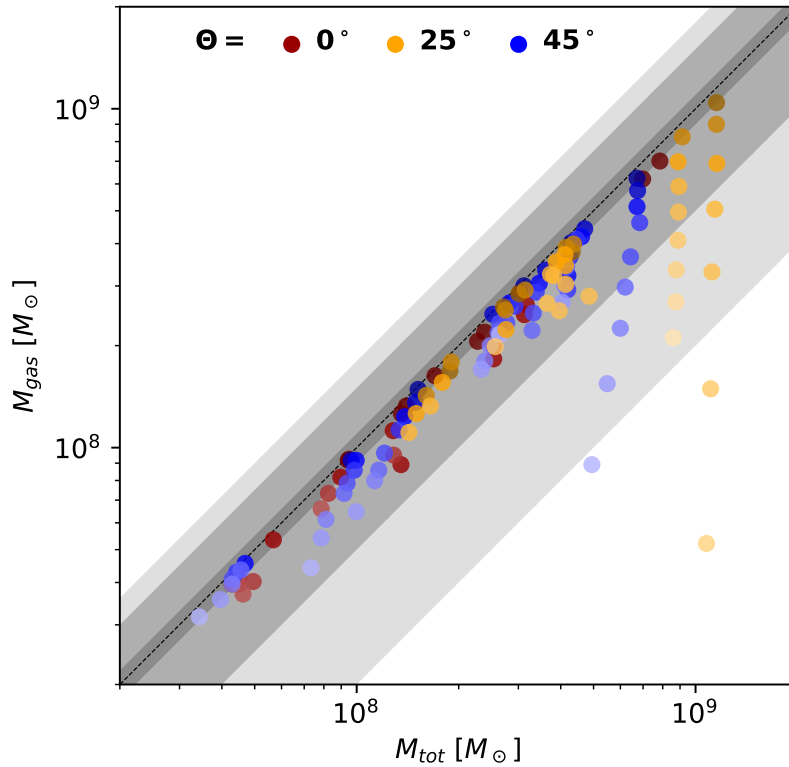

Figure 4.7: Gas mass vs. total mass of stripped dwarfs galaxies. The dashed black line indicates a 1:1 relationship, while the grey contours represent a 10%, 50% and 80% decline.

4.7   Radial Shrink

Figure 4.8 shows the dwarfs' evolution tracks in the stellar mass vs. gas mass plane over a period of ~ 1.5 Gyr with a time step of ~ 0.5 Gyr between evaluations. The grey horizontal line indicates a resolution threshold of five stellar particles, while the blue and red arrows indicate dwarfs from the elliptical ($\Theta = 45°$) and radial ($\Theta = 0°$) merger orbit case respectively. In principle, the gas content of a dwarf can decrease in two ways - it either is converted into stars or it is stripped by the environment. The former case implies that the

sum of the gas and stellar mass will stay constant, which is represented by the black contours. Therefore, dwarfs will follow these lines if they are not experiencing gas stripping and decline to the left with respect to the contours if they lose gas mass to the environment. Meanwhile, the stellar mass of the dwarfs keeps rising, which becomes apparent by looking at the right plot of Figure 4.8. As in the left hand side plot, it again shows the stellar mass on the y-axis, but this time against the stellar half mass radius on the x-axis. The color coding is the same as before, whereas the contours indicate linearly increasing mean stellar density, i.e. we have $\rho_* \propto M_*/r^3_{*,1/2} = const.$ along a contour line.
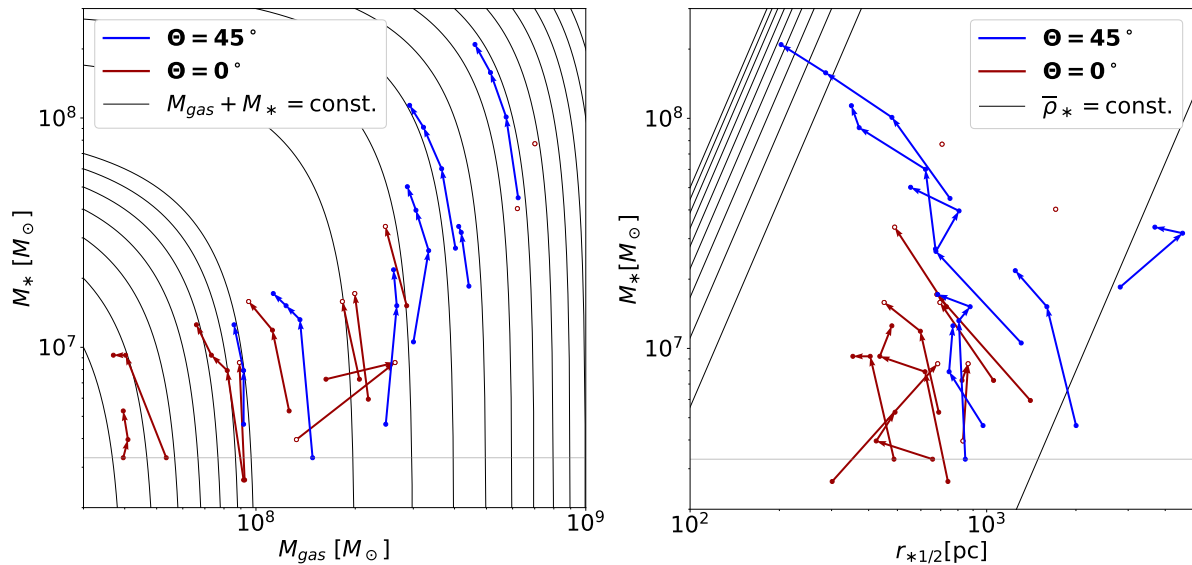

Figure 4.8: Time evolution of simulated tidal dwarfs forming due to galaxy merger on an elliptical (blue) and radial (red) orbit in a cluster. Traced over 1.5 Gyr, with $\Delta t \sim 0.5$ Gyr. Open circles indicate that the dwarf was destroyed afterwards. The grey horizontal line indicates a threshold of five stellar particles. *Left*: Gas mass vs. stellar mass. Tracks follow contours if no gas is stripped. *Right*: Stellar half-mass radius vs. stellar mass. Contours indicate linearly increasing $\overline{\rho}_*$. The outlier with large half mass radii is in fact a bound dwarf double system.

Although their stellar mass keeps rising, almost all dwarfs decrease their stellar radius over time, as already mentioned in the previous section (cf Figure 4.6). I argue that the decreasing stellar half mass radii are a consequence of the ongoing gas compression, which forces the gas to become compact and in turn restricts the stellar extent, since the stars need to follow the gravitational potential dominated by the gas. This is also supported by the fact that many of the analysed dwarfs display a leading tail of stars, which were previously traced to be in the corresponding dwarf galaxy (cf. Figure 4.3). Since the total mass is dominated by the gas, the dwarfs' dynamical behaviour will be governed by forces acting on this component. Consequently, the movement of a dwarf through the cluster is slowed down by the intracluster gas. Stars, on the other hand, do not experience ram pressure. These stars, which are at a larger distance to the dwarf centre, are therefore more prone to escape its potential in the opposite direction from which ram pressure is pushing on the gaseous dwarf. As a result, the dwarfs can only keep stars at their very centre, which results in small stellar half mass radii.

4.8   Time Evolution in Detail

Figure 4.9 demonstrates the time evolution of the gas mass M_{gas}, stellar mass M_*, clustercentric distance D_{Cluster} and distance to the merger remnant D_{gal} of the three simulated scenarios with cluster infall angles $\Theta = 0°$ (red), $\Theta = 25°$ (orange) and $\Theta = 45°$ (blue). Open circles indicate that the dwarf galaxy was not present anymore at the subsequent tracing time. Dwarfs forming in the wake of a galaxy merger moving radially towards the cluster (B0) do not survive longer that ~1.5 Gyr because they reach the cluster centre at that point. Comparing the left-hand side panels with each other, we see a clear trend of decreasing gas masses, while the stellar masses rise due to active star formation. The abrupt decline in stellar mass of some dwarfs is explained by close passage and hence tidal stripping by the cluster centre, after which many are destroyed. The other disrupted dwarfs in that sample do not show the decline in stellar mass because they are destroyed much quicker due to their lower initial mass, which is not resolved in this tracing with coarse time steps of ~0.5 Gyr. While the merger remnant is moving on a splashback orbit, most tidal dwarfs continue to spiral into the cluster for the two elliptical cases. After 4 Gyr, there are still 3 and 4 dwarf galaxies present for the two elliptical orbit scenarios B25 and B45, respectively. At this point, they have already reached large distances in the order of the cluster's virial radius to their progenitor (cf. third panel in Figure 4.9). These showcases demonstrate that isolated dwarf galaxies in clusters can be of tidal origin and be present for a significant fraction of the
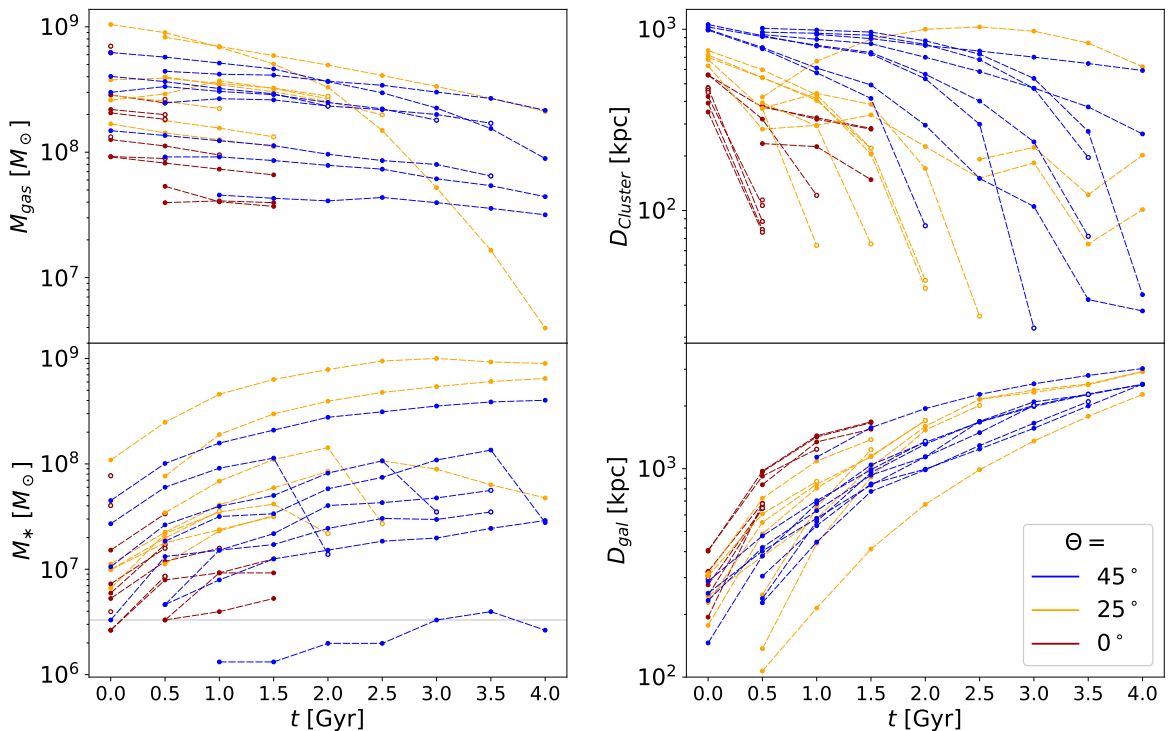

Figure 4.9: Time evolution of stripped tidal dwarfs forming due to a galaxy merger on three different orbits in a cluster. Open circles indicate that the dwarf is destroyed afterwards due to close passage by the cluster centre. The grey horizontal line in the bottom left figure represents a threshold of five stellar particles.

Hubble time.

Each of the two elliptical cases B25 and B45 displays a noticable outlier at the high gas mass end, which convert gas into stars with exceptionally higher rates. Their large size facilitates the formation of cold, star forming clouds embedded in the dwarf galaxy, which is surrounded by hot intracluster medium, while also stabilizing the dwarf against tidal shear in the cluster as well. There is another different peculiar object – a dwarf in the B25 configuration – whose stellar and gas component is sheared into two separate objects after $t = 2$ Gyr. At that point, is has reached a stellar mass of $\sim 2 \times 10^8$ $M_\odot$. One of the descendant is completely made out of stars and continues to be present in the cluster, whereas the other inherits the available gas mass reservoir but evaporates after $t = 2.5$ Gyr.

Contribution of Tidal Dwarf Galaxies to Dwarf Population

While early studies estimated that all dwarf galaxies could be of tidal origin (Okazaki & Taniguchi, 2000), follow-up surveys deduced much smaller fractions: 16% in the observational sample of Sweet et al. (2014), 10% by Bournaud & Duc (2006) in which the authors simulated isolated galaxy major mergers, and even as low as 6% by Kaviraj et al. (2012), who performed a statistical observational investigation of tidal dwarf galaxies in the local Universe. The latter study employed the result of Bournaud & Duc (2006), that in conditions favorable for tidal dwarf formation – being wet, prograde major mergers with mass ratios between 1:1-4:1 and incline between the two orbital planes ≤40° – only 1-2 massive ($M > 10^8 M_\odot$) tidal dwarfs per merging galaxy survive for at least 1 Gyr. However, this conclusion can be only valid in case of a negligible environment, since the simulation sample consists of isolated galaxy mergers. The main reason for the low number of tidal dwarfs per merger in their study is that the only structures able to survive for a long period of time, are those which have high initial masses and form far enough away from the progenitor galaxies, such that they are not disrupted by the parents' tidal field. In this chapter, I have shown that the number of massive tidal dwarf galaxies formed by a major merger can be significantly higher when environmental interaction is taken into account. Since the aim was a proof of concept using three exemplary orbit configurations, my dwarf production rate is not a robust statistical prediction. Still, to demonstrate the potential increase of the true tidal dwarf galaxy fraction in the local Universe, I repeat the estimation performed in Section 6 by Kaviraj et al. (2012), but using the dwarf formation rate from my simulations.

The observational sample studied by Kaviraj et al. (2012) suggests that only ~18% of wet major mergers produce tidal dwarf galaxies. In conditions which allow long-lived tidal dwarfs – i.e. no radial infall and thus no rapid tidal disruption by the cluster – I produce ~6.5 stable (present for >1 Gyr), massive ($M > 10^8 M_\odot$) tidal dwarf galaxies in the configurations C45 (6 dwarfs) and C25 (7 dwarfs), respectively. Hence I estimate that $0.18 \times 6.5 = $ *1.17 tidal dwarfs form per wet, major merger event*. By integrating an empirically motivated major merger rate, Conselice (2007) concluded that each massive galaxy experiences ~4 major mergers in its lifetime. Since early interactions before $z = 1$ are expected to be dominated by gas-rich

galaxies (e.g. Kaviraj et al., 2009) and at most one major merger usually happens after that time (e.g. Conselice et al., 2003a; Lin et al., 2004; Jogee et al., 2009), this indicates that, statistically, a massive galaxy experiences ~3 wet, major mergers. Considering earlier works (Bournaud, 2010), which found that ~50% of massive tidal dwarf galaxies (i.e. $M > 10^8 M_\odot$) survive a significant fraction of the Hubble time – i.e. present for several Gyr – I arrive at $3 \times 0.5 \times 1.17 = $ *1.76 long-lived tidal dwarfs per massive galaxy*. The observed galaxy mass function of the Coma cluster (Secker & Harris, 1996) suggests a ratio between dwarf galaxies with $M > 10^8 M_\odot$ to massive galaxies of ~5.8. Using this value, I therefore conclude that the ratio of tidal galaxies among dwarfs in clusters could be as high as ~30% (= 1.76/5.8).

I stress that several oversimplifying assumptions entered into this estimate. As pointed out by Kaviraj et al. (2012), this approach assumes a constant tidal dwarf production rate over cosmic time, even though mergers at higher redshift are expected to be more gas-rich, amplifying the probability of forming tidal dwarf galaxies. Moreover, I assessed the probability (namely ~50%) of the dwarfs' long-time survival by applying the statistical result from the isolated merger simulations of Bournaud & Duc (2006), in which the reason for short lifetimes was tidal disruption by the progenitor. Although the limiting factor in my sample is the hostile cluster environment, the survival fraction in my simulations is still in a similar range. Finally, the orbit of the galaxy merger in the cluster was also not taken into account. It determines both the survival rate of tidal dwarfs getting destroyed in the cluster centre, as well as the impact angle between the tidal tails and the direction of ram pressure, which lead to a different number of gaseous dwarf galaxies per merger being able to escape the parents' gravitational potential. Nevertheless, my results demonstrate that – within these plain assumptions – the tidal dwarf fraction is most probably higher than currently adopted in the literature.

Summary and Conclusion

The goal of this thesis was to test the viability of environmentally driven tidal dwarf formation by galaxy mergers in clusters and to examine if such low-mass objects could be stripped from their progenitor, thus populating the cluster with isolated dwarf galaxies. First, I layed the groundwork in Chapter 2 by investigating the evolution of isolated major mergers. In particular, I searched for configurations producing extended tidal tails of gas such as in the well observed merger in cluster Abell 3574, involving NGC 5291 and the Seashell galaxy. Varying the orbit and properties of the simulated galaxies, I find prograde, gas-rich mergers with large impact angles to be promising candidates for reproducing the aforementioned constellation. Since this work was mainly concerned with the formation of small stellar associations, I tested whether the simulated star formation activity was increasing with improved resolution, but found no such correlation for the tested values in the high-resolution range. To demonstrate the variety of possible tidal morphologies, I finally compiled a catalog with the time evolution of 70 simulated galaxy mergers, varying the impact angle and orientation of the galactic discs.

Thereafter, I initialized a galaxy cluster consisting of a dark matter halo and hot gaseous atmosphere in Chapter 3 and ensured its numerical stability. Placing a galaxy merger into such an environment yielded substantially altered results compared to the isolated cases tested beforehand. Exposed to ram pressure, the tidal gas condenses into thin, compact tails, triggering a remarkably high star formation rate across the entire tidal complex. Eventually, the continued environmental influence indeed caused the young tidal dwarf galaxies to escape from their progenitor's potential.

Chapter 4 was dedicated to the detailed analysis of the formation and evolution of such stripped tidal dwarf galaxies. To this end I conducted three simulations, initializing a galaxy merger in a cluster with varying impact angle towards the cluster centre. All three configurations produce such isolated low-mass objects. Decoupled from their cradle, the dwarf galaxies begin to evolve independently, increasing their distances to the merger remnant up to ~Mpc. Since they originate from the tidal tail of the merger, these stripped tidal dwarfs are generally dark matter deficient, i.e., the gas component dominates their total mass. The gas and stellar mass range of the found dwarfs is $M_{\mathrm{gas}} \approx 10^7 - 10^9 \, M_\odot$ and $M_* \approx 10^6 - 10^8 \, M_\odot$, respectively, while the stellar half mass radii typically lie between $r_{*1/2} \approx 10^2 - 10^3$ pc.

Moving through the ICM, these objects continue to exhibit high star formation rates due to ram pressure, while curiously decreasing their stellar half mass radii, resulting in diverse dwarf galaxy types. I traced the evolution of the stripped tidal dwarfs over a time period of ~4 Gyr after the merger event, in which the dwarf galaxies spiral towards the cluster centre with varying tempo. With time, they either evaporate due to their low initial mass, or are disrupted by tidal fields as soon as they reach the cluster centre. However, there are still intact dwarf galaxies present even ~4 Gyr after the merger event, having clustercentric distances in the order of 10 kpc to a few 100 kpc. This finding demonstrates that such objects can prevail for a significant fraction of the Hubble time.

Compared to the isolated merger simulations by Bournaud & Duc (2006), the experiments presented in this work produce a significantly higher tidal dwarf production rate due to environmental interaction. To evaluate the resulting contribution on the total dwarf population, I compared this tidal dwarf production rate to the observed galaxy mass function in clusters in Chapter 5. According to this calculation, the fraction of dwarf galaxies with tidal origin could be in the order of ~30%. That value is significantly higher than in currently adopted estimates by the literature, since the latter do not consider environmentally supported formation scenarios.
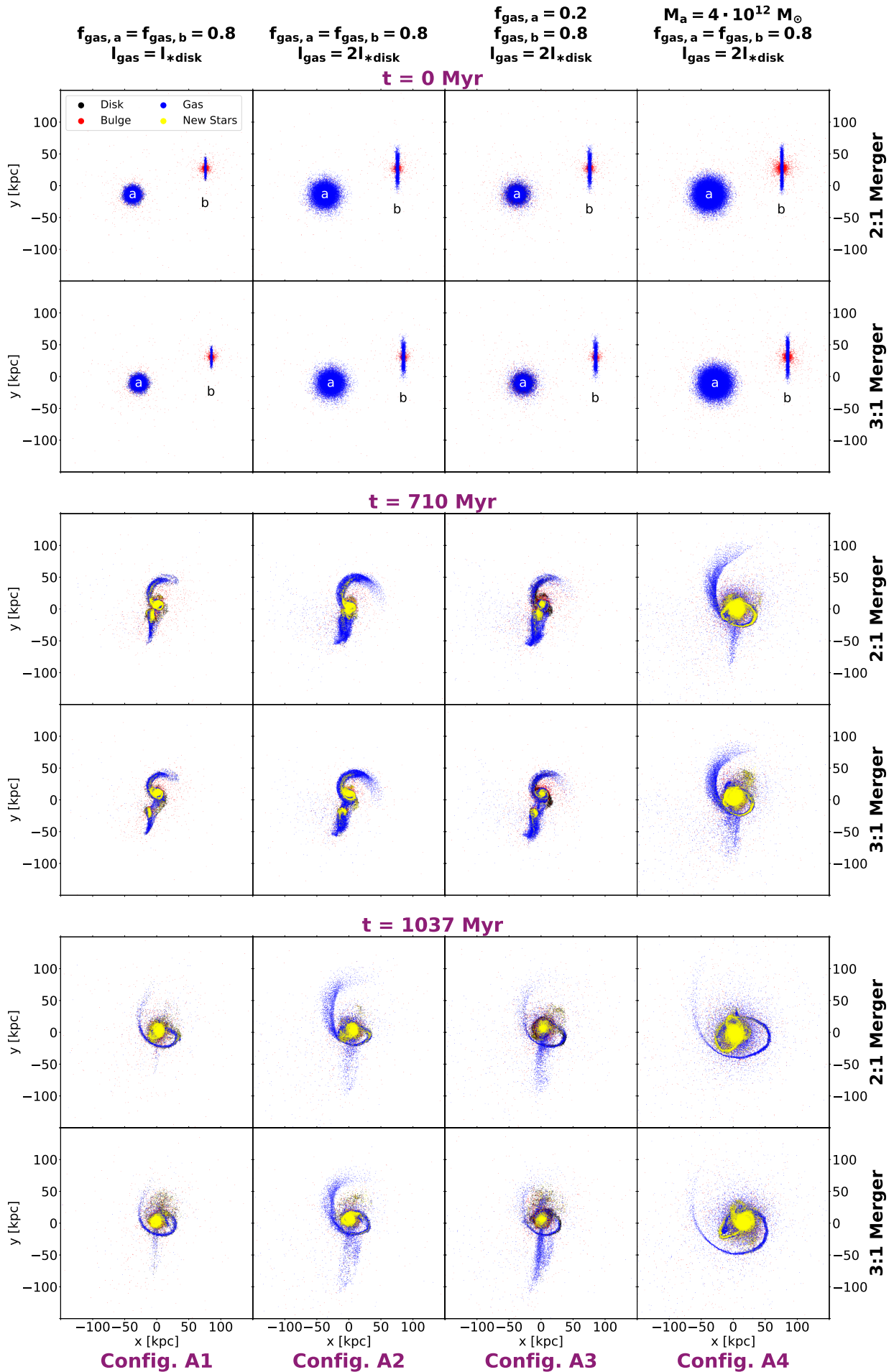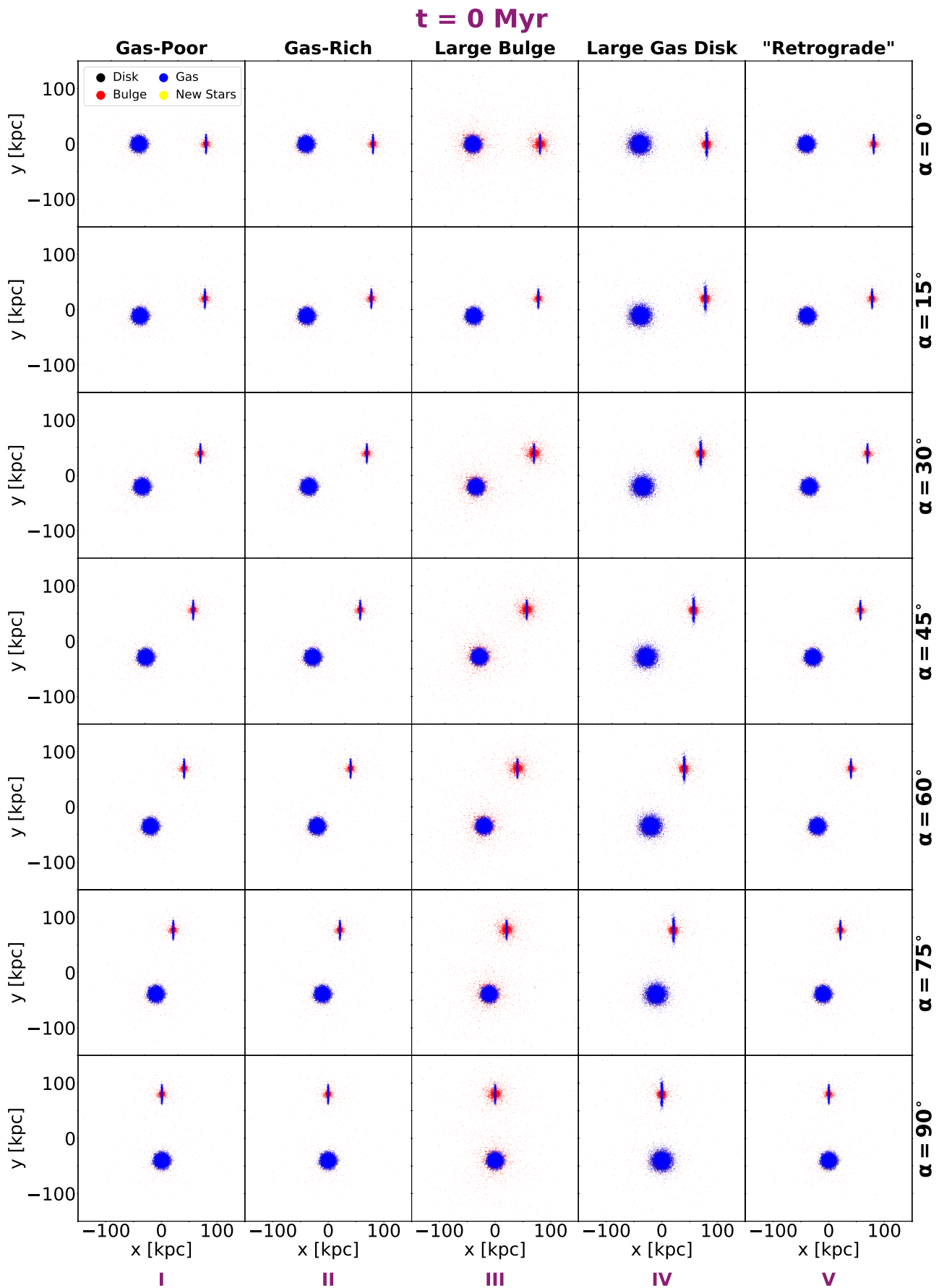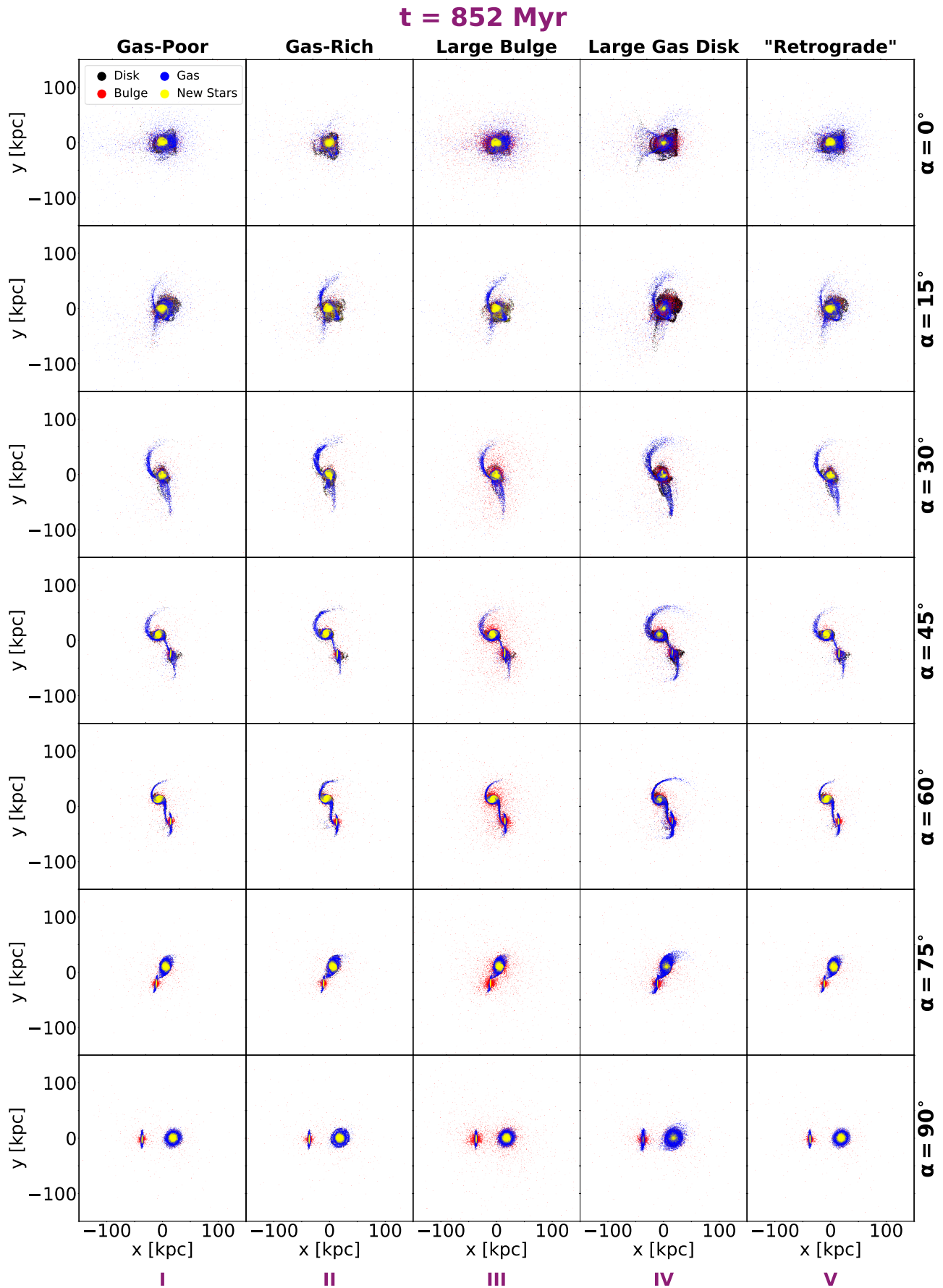
Appendix

Figure A1: Morphological differences arising by implementing different galaxy properties. This figure is the counterpart to Figure 2.6, implementing a different orbit.

Figure A2: Variance of galaxy properties and impact angle in a 2:1 merger with perpendicular disks. This figure is the counterpart to Figure 2.8a, implementing a different orbit.

(a) Initial conditions for merger catalog.

Figure A2: Variance of galaxy properties and impact angle in a 2:1 merger with perpendicular disks. This figure is the counterpart to Figure 2.8b, implementing a different orbit.

(b) Time evolution of initial conditions in Figure A2a.

Figure A2: Variance of galaxy properties and impact angle in a 2:1 merger with perpendicular disks. This figure is the counterpart to Figure 2.8c, implementing a different orbit.
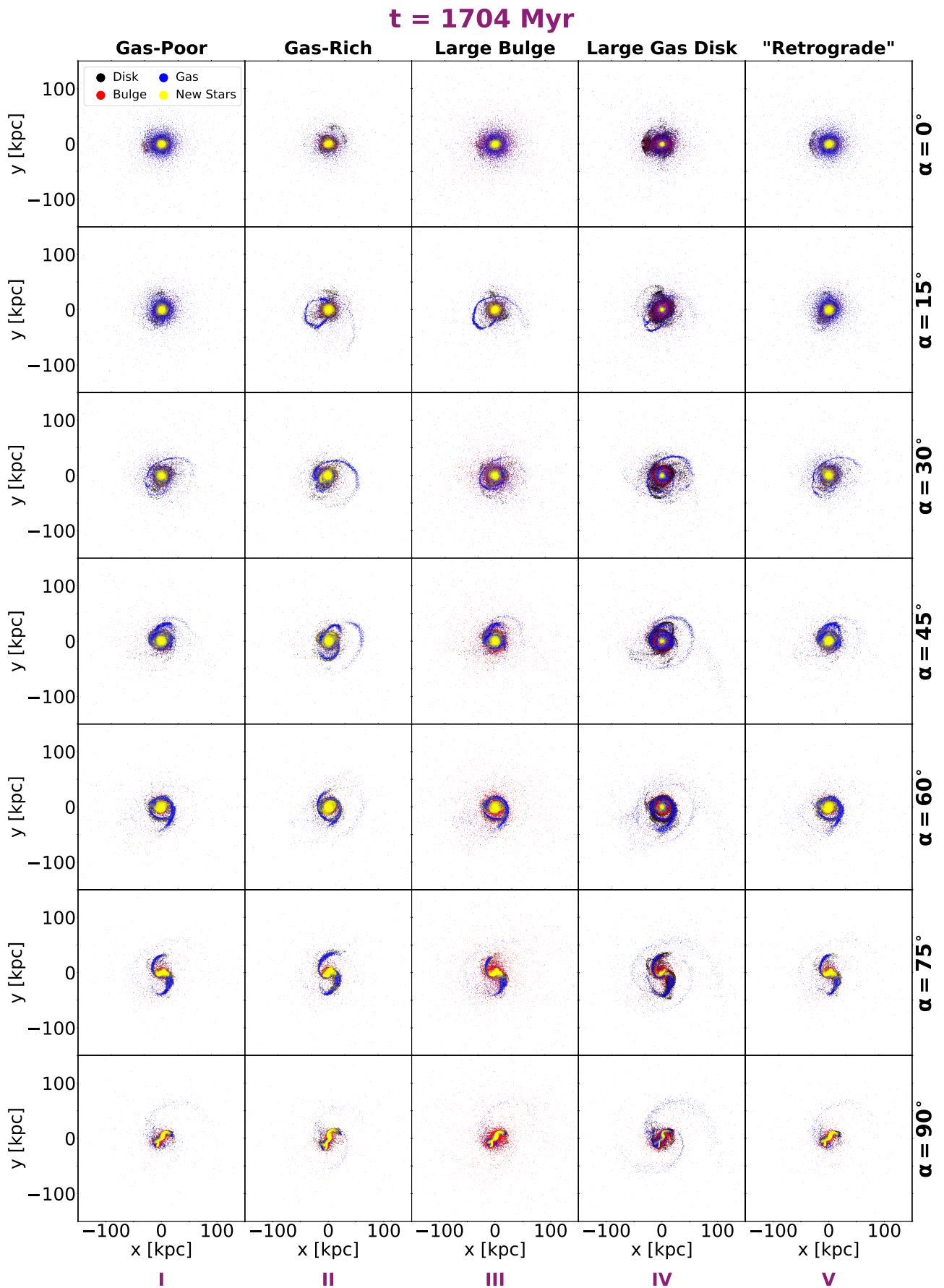

(c) Time evolution of initial conditions in Figure A2a.

Figure A2: Variance of galaxy properties and impact angle in a 2:1 merger with perpendicular disks. This figure is the counterpart to Figure 2.8d, implementing a different orbit.
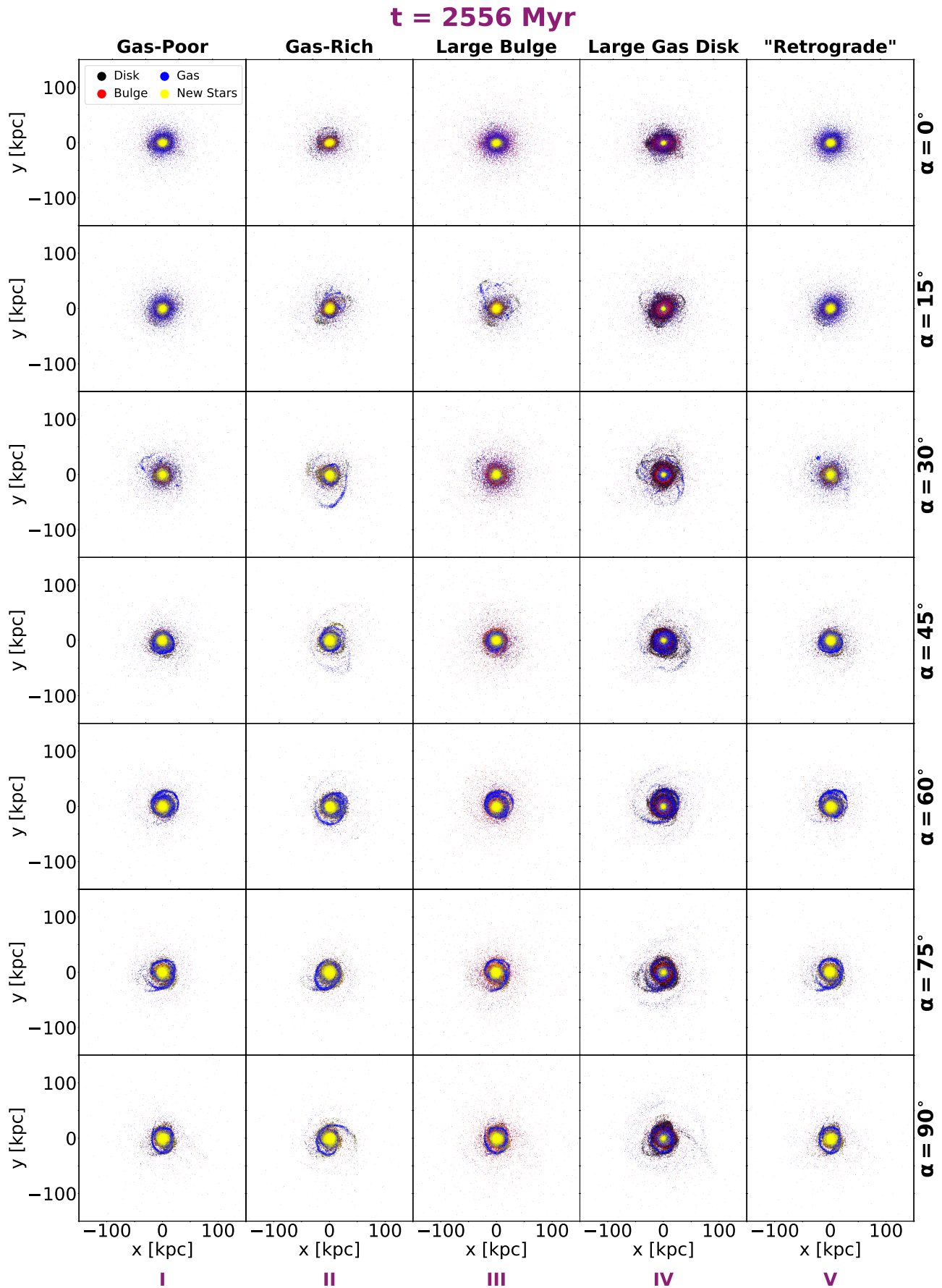

(d) Time evolution of initial conditions in Figure A2a.

References

Agertz, O., Moore, B., Stadel, J., et al. (2007). Fundamental differences between SPH and grid methods. MNRAS, 380, 963–978.

Appel, A. W. (1985). An Efficient Program for Many-Body Simulation. SIAM Journal on Scientific and Statistical Computing, 6, 85–103.

Baldry, I. K., Driver, S. P., Loveday, J., et al. (2012). Galaxy And Mass Assembly (GAMA): the galaxy stellar mass function at z < 0.06. MNRAS, 421, 621–634.

Barnes, J. & Hut, P. (1986). A hierarchical O(N log N) force-calculation algorithm. Nature, 324, 446–449.

Barnes, J. E. & Hernquist, L. (1992). Formation of dwarf galaxies in tidal tails. Nature, 360, 715–717.

Beck, A. M., Murante, G., Arth, A., et al. (2016). An improved SPH scheme for cosmological simulations. MNRAS, 455, 2110–2130.

Binney, J. & Tremaine, S. (2008). Galactic Dynamics: Second Edition.

Bondi, H. (1952). On spherically symmetrical accretion. MNRAS, 112, 195.

Bournaud, F. (2010). Tidal dwarf galaxies and missing baryons. Advances in Astronomy, 2010, 1–7.

Bournaud, F., Bois, M., Emsellem, E., & Duc, P. A. (2008). Galaxy mergers at high resolution: From elliptical galaxies to tidal dwarfs and globular clusters. Astronomical Notes, 329, 1025–1028.

Bournaud, F. & Duc, P. A. (2006). From tidal dwarf galaxies to satellite galaxies. A&A, 456, 481–492.

Briggs, F. H., Wolfe, A. M., Krumm, N., & Salpeter, E. E. (1980). First results of a sensitive search for H I envelopes in a complete sample of spiral galaxies : extensive H I near the isolated SC I NGC 628. ApJ, 238, 510–523.

Brodie, J. P., Romanowsky, A. J., Strader, J., & Forbes, D. A. (2011). The Relationships among Compact Stellar Systems: A Fresh View of Ultracompact Dwarfs. AJ, 142, 199.

Bryan, G. L. & Norman, M. L. (1998). Statistical Properties of X-Ray Clusters: Analytic and Numerical Comparisons. ApJ, 495, 80–99.

Burkert, A. & Naab, T. (2003). Major Mergers and the Origin of Elliptical Galaxies. In G. Contopoulos, & N. Voglis (Eds.) *Galaxies and Chaos*, vol. 626, pp. 327–339.

Cavaliere, A. & Fusco-Femiano, R. (1978). The Distribution of Hot Gas in Clusters of Galaxies. A&A, 70, 677.

Chabrier, G. (2003). Galactic Stellar and Substellar Initial Mass Function. PASP, 115, 763–795.

Choudhuri, A. R. (1998). The physics of fluids and plasmas: an introduction for astrophysicists.

Cohen, Y., van Dokkum, P., Danieli, S., et al. (2018). The Dragonfly Nearby Galaxies Survey. V. HST/ACS Observations of 23 Low Surface Brightness Objects in the Fields of NGC 1052, NGC 1084, M96, and NGC 4258. ApJ, 868, 96.

Conselice, C. J. (2007). Galaxy Mergers and Interactions at High Redshift. In F. Combes, & J. Palouš (Eds.) *Galaxy Evolution across the Hubble Time*, vol. 235. pp. 381–384.

Conselice, C. J., Bershady, M. A., Dickinson, M., & Papovich, C. (2003a). A Direct Measurement of Major Galaxy Mergers at z<~3. AJ, 126, 1183–1207.

Conselice, C. J., Gallagher, John S., I., & Wyse, R. F. G. (2003b). Galaxy Populations and Evolution in Clusters. III. The Origin of Low-Mass Galaxies in Clusters: Constraints from Stellar Populations. AJ, 125, 66–85.

Croston, J. H., Pratt, G. W., Böhringer, H., et al. (2008). Galaxy-cluster gas-density distributions of the representative XMM-Newton cluster structure survey (REXCESS). A&A, 487, 431–443.

Danieli, S., van Dokkum, P., Conroy, C., Abraham, R., & Romanowsky, A. J. (2019). Still Missing Dark Matter: KCWI High-resolution Stellar Kinematics of NGC1052-DF2. ApJ, 874, L12.

Dehnen, W. & Aly, H. (2012). Improving convergence in smoothed particle hydrodynamics simulations without pairing instability. MNRAS, 425, 1068–1082.

Dolag, K., Reinecke, M., Gheller, C., & Imboden, S. (2008). Splotch: visualizing cosmological simulations. New Journal of Physics, 10, 125006.

Donnert, J. M. F. (2014). Initial conditions for idealized clusters mergers, simulating 'El Gordo'. MNRAS, 438, 1971–1984.

Drinkwater, M. J., Jones, J. B., Gregg, M. D., & Phillipps, S. (2000). Compact Stellar Systems in the Fornax Cluster: Super-massive Star Clusters or Extremely Compact Dwarf Galaxies? PASA, 17, 227–233.

Dubinski, J. (1998). The Origin of the Brightest Cluster Galaxies. ApJ, 502, 141–149.

Duc, P.-A. (2012). Birth, Life and Survival of Tidal Dwarf Galaxies. In *Dwarf Galaxies: Keys to Galaxy Formation and Evolution*, vol. 28 of *Astrophysics and Space Science Proceedings*. p. 305.

Duc, P. A., Cayatte, V., Balkowski, C., et al. (2001). H I-rich dwarf galaxies in the Hydra I cluster. II. Spectroscopic data. A&A, 369, 763–777.

Duc, P. A. & Mirabel, I. F. (1998). Young tidal dwarf galaxies around the gas-rich disturbed lenticular NGC 5291. A&A, 333, 813–826.

Friedmann, A. (1922). Über die Krümmung des Raumes. Zeitschrift fur Physik, 10, 377–386.

Gannon, J. S., Forbes, D. A., Romanowsky, A. J., et al. (2020). On the stellar kinematics and mass of the Virgo ultradiffuse galaxy VCC 1287. MNRAS, 495, 2582–2598.

Gerhard, O. E. (1981). N-body simulations of disc-halo galaxies - Isolated systems, tidal interactions and merging. MNRAS, 197, 179–208.

Gray, L. M., Rhode, K. L., Leisman, L., et al. (2023). Catching Tidal Dwarf Galaxies at a Later Evolutionary Stage with ALFALFA. AJ, 165, 197.

Guo, Q., Hu, H., Zheng, Z., et al. (2020). Further evidence for a population of dark-matter-deficient dwarf galaxies. Nature Astronomy, 4, 246–251.

Hammer, F., Yang, Y., Arenou, F., et al. (2020). Orbital Evidences for Dark-matter-free Milky Way Dwarf Spheroidal Galaxies. ApJ, 892, 3.

Haslbauer, M., Dabringhausen, J., Kroupa, P., Javanmardi, B., & Banik, I. (2019). Galaxies lacking dark matter in the Illustris simulation. A&A, 626, A47.

Hau, G. K. T., Carter, D., & Balcells, M. (1999). The shell elliptical galaxy NGC 2865: evolutionary population synthesis of a kinematically distinct core. MNRAS, 306, 437–460.

Hernquist, L. (1990). An Analytical Model for Spherical Galaxies and Bulges. ApJ, 356, 359.

Hubble, E. (1929). A Relation between Distance and Radial Velocity among Extra-Galactic Nebulae. Proceedings of the National Academy of Science, 15, 168–173.

Hubble, E. P. (1936). Realm of the Nebulae.

Iglesias-Páramo, J., van Driel, W., Duc, P. A., et al. (2003). A study of H I-selected galaxies in the Hercules cluster. A&A, 406, 453–469.

Jackson, R. A., Kaviraj, S., Martin, G., et al. (2021). Dark matter-deficient dwarf galaxies form via tidal stripping of dark matter in interactions with massive companions. MNRAS, 502, 1785–1796.

Jing, Y., Wang, C., Li, R., et al. (2019). Dark-matter-deficient galaxies in hydrodynamical simulations. MNRAS, 488, 3298–3307.

Jogee, S., Miller, S. H., Penner, K., et al. (2009). History of Galaxy Interactions and Their Impact on Star Formation Over the Last 7 Gyr from GEMS. ApJ, 697, 1971–1992.

Jones, M. G., Karunakaran, A., Bennet, P., et al. (2023). Gas-rich, Field Ultra-diffuse Galaxies Host Few Gobular Clusters. ApJ, 942, L5.

Kapferer, W., Sluka, C., Schindler, S., Ferrari, C., & Ziegler, B. (2009). The effect of ram pressure on the star formation, mass distribution and morphology of galaxies. A&A, 499, 87–102.

Karademir, G. S., Remus, R.-S., Burkert, A., et al. (2019). The outer stellar halos of galaxies: how radial merger mass deposition, shells, and streams depend on infall-orbit configurations. MNRAS, 487, 318–332.

Katz, N., Weinberg, D. H., & Hernquist, L. (1996). Cosmological Simulations with TreeSPH. ApJS, 105, 19.

Kaviraj, S., Darg, D., Lintott, C., Schawinski, K., & Silk, J. (2012). Tidal dwarf galaxies in the nearby Universe. MNRAS, 419, 70–79.

Kaviraj, S., Peirani, S., Khochfar, S., Silk, J., & Kay, S. (2009). The role of minor mergers in the recent star formation history of early-type galaxies. MNRAS, 394, 1713–1720.

Kazantzidis, S., Moore, B., & Mayer, L. (2004). Galaxies and Overmerging: What Does It Take to Destroy a Satellite Galaxy? In F. Prada, D. Martinez Delgado, & T. J. Mahoney (Eds.) *Satellites and Tidal Streams*, vol. 327 of *Astronomical Society of the Pacific Conference Series*. p. 155.

Kroupa, P. (2012). The Dark Matter Crisis: Falsification of the Current Standard Model of Cosmology. PASA, 29, 395–433.

Lee, J., Kimm, T., Blaizot, J., et al. (2022). Simulating Jellyfish Galaxies: A Case Study for a Gas-rich Dwarf Galaxy. ApJ, 928, 144.

Lee, J., Shin, E.-j., & Kim, J.-h. (2021). Dark Matter Deficient Galaxies and Their Member Star Clusters Form Simultaneously during High-velocity Galaxy Collisions in 1.25 pc Resolution Simulations. ApJ, 917, L15.

Li, C. & White, S. D. M. (2009). The distribution of stellar mass in the low-redshift Universe. MNRAS, 398, 2177–2187.

Lin, L., Koo, D. C., Willmer, C. N. A., et al. (2004). The DEEP2 Galaxy Redshift Survey: Evolution of Close Galaxy Pairs and Major-Merger Rates up to z ~1.2. ApJ, 617, L9–L12.

Mancera Piña, P. E., Fraternali, F., Adams, E. A. K., et al. (2019). Off the Baryonic Tully-Fisher Relation: A Population of Baryon-dominated Ultra-diffuse Galaxies. ApJ, 883, L33.

Martin, G., Bazkiaei, A. E., Spavone, M., et al. (2022). Preparing for low surface brightness science with the Vera C. Rubin Observatory: Characterization of tidal features from mock images. MNRAS, 513, 1459–1487.

Martin, M. C. (1998). Catalogue of HI maps of galaxies. II. Analysis of the data. A&AS, 131, 77–87.

Mastropietro, C. & Burkert, A. (2008). Simulating the Bullet Cluster. MNRAS, 389, 967–988.

Mieske, S., Infante, L., Benítez, N., et al. (2004). Ultracompact Dwarf Galaxies in Abell 1689: A Photometric Study with the Advanced Camera for Surveys. AJ, 128, 1529–1540.

Mirabel, I. F., Dottori, H., & Lutz, D. (1992). Genesis of a dwarf galaxy from the debris of the Antennae. A&A, 256, L19–L22.

Moles, M., Marquez, I., & Sulentic, J. W. (1998). The observational status of Stephan's Quintet. A&A, 334, 473–481.

Mukhanov, V. (2005). Physical Foundations of Cosmology.

Navarro, J. F., Frenk, C. S., & White, S. D. M. (1997). A Universal Density Profile from Hierarchical Clustering. ApJ, 490, 493–508.

Niemiec, A., Jullo, E., Giocoli, C., Limousin, M., & Jauzac, M. (2019). Dark matter stripping in galaxy clusters: a look at the stellar-to-halo mass relation in the Illustris simulation. MNRAS, 487, 653–666.

Nussbaumer, H. & Bieri, L. (2011). Who discovered the expansion of the Universe? The Observatory, 131, 394–398.

Ogiya, G. (2018). Tidal stripping as a possible origin of the ultra diffuse galaxy lacking dark matter. MNRAS, 480, L106–L110.

Oh, S., Kim, K., Lee, J. H., et al. (2018). KYDISC: Galaxy Morphology, Quenching, and Mergers in the Cluster Environment. ApJS, 237, 14.

Okazaki, T. & Taniguchi, Y. (2000). Dwarf Galaxy Formation Induced by Galaxy Interactions. ApJ, 543, 149–152.

Otaki, K. & Mori, M. (2023). Frequency of the dark matter subhalo collisions and bifurcation sequence arising formation of dwarf galaxies. MNRAS, 525, 2535–2552.

Planck Collaboration, Aghanim, N., Akrami, Y., et al. (2020). Planck 2018 results. I. Overview and the cosmological legacy of Planck. A&A, 641, A1.

Ploeckinger, S., Sharma, K., Schaye, J., et al. (2018). Tidal dwarf galaxies in cosmological simulations. MNRAS, 474, 580–596.

Poggianti, B. M., Bridges, T. J., Mobasher, B., et al. (2001). A Photometric and Spectroscopic Study of Dwarf and Giant Galaxies in the Coma Cluster. III. Spectral Ages and Metallicities. ApJ, 562, 689–712.

Rakhi, R., Santhosh, G., Joseph, P., et al. (2023). UVIT view of NGC 5291: Ongoing star formation in tidal dwarf galaxies at 0.35 kpc resolution. MNRAS, 522, 1196–1207.

Rakos, K. D., Schombert, J. M., Odell, A. P., & Steindling, S. (2000). Cluster Populations in A115 and A2283. ApJ, 540, 715–725.

Reaves, G. (1956). Dwarf galaxies in the Virgo cluster. AJ, 61, 69–76.

Remus, R.-S., Burkert, A., Dolag, K., et al. (2013). The Dark Halo—Spheroid Conspiracy and the Origin of Elliptical Galaxies. ApJ, 766, 71.

Román, J., Jones, M. G., Montes, M., et al. (2021). A diffuse tidal dwarf galaxy destined to fade out as a "dark galaxy". A&A, 649, L14.

Sabatini, S., Davies, J., Scaramella, R., et al. (2003). The dwarf LSB galaxy population of the Virgo cluster - I. The faint-end slope of the luminosity function. MNRAS, 341, 981–992.

Sandage, A. (1961). The Hubble Atlas of Galaxies.

Schaye, J., Crain, R. A., Bower, R. G., et al. (2015). The EAGLE project: simulating the evolution and assembly of galaxies and their environments. MNRAS, 446, 521–554.

Secker, J. & Harris, W. E. (1996). The Early-Type Dwarf-to-Giant Ratio and Substructure in the Coma Cluster. ApJ, 469, 623.

Sextl, E., Kudritzki, R.-P., Zahid, H. J., & Ho, I. T. (2023). Mass-Metallicity Relationship of SDSS Star-forming Galaxies: Population Synthesis Analysis and Effects of Star Burst Length, Extinction Law, Initial Mass Function, and Star Formation Rate. ApJ, 949, 60.

Shin, E.-j., Jung, M., Kwon, G., et al. (2020). Dark Matter Deficient Galaxies Produced via High-velocity Galaxy Collisions in High-resolution Numerical Simulations. ApJ, 899, 25.

Silk, J. (2019). Ultra-diffuse galaxies without dark matter. MNRAS, 488, L24–L28.

Springel, V. (2005). The cosmological simulation code GADGET-2. MNRAS, 364, 1105–1134.

Springel, V., Di Matteo, T., & Hernquist, L. (2005). Modelling feedback from stars and black holes in galaxy mergers. MNRAS, 361, 776–794.

Springel, V. & Hernquist, L. (2003). Cosmological smoothed particle hydrodynamics simulations: a hybrid multiphase model for star formation. MNRAS, 339, 289–311.

Sweet, S. M., Drinkwater, M. J., Meurer, G., et al. (2014). Choirs H I Galaxy Groups: The Metallicity of Dwarf Galaxies. ApJ, 782, 35.

Teyssier, R., Chapon, D., & Bournaud, F. (2010). The Driving Mechanism of Starbursts in Galaxy Mergers. ApJ, 720, L149–L154.

Tonnesen, S. & Bryan, G. L. (2021). It's Cloud's Illusions I Recall: Mixing Drives the Acceleration of Clouds from Ram Pressure Stripped Galaxies. ApJ, 911, 68.

Toomre, A. & Toomre, J. (1972). Galactic Bridges and Tails. ApJ, 178, 623–666.

van Dokkum, P., Danieli, S., Abraham, R., Conroy, C., & Romanowsky, A. J. (2019). A Second Galaxy Missing Dark Matter in the NGC 1052 Group. ApJ, 874, L5.

van Dokkum, P., Danieli, S., Cohen, Y., et al. (2018). A galaxy lacking dark matter. Nature, 555, 629–632.

van Dokkum, P., Shen, Z., Keim, M. A., et al. (2022). A trail of dark-matter-free galaxies from a bullet-dwarf collision. Nature, 605, 435–439.

van Dokkum, P. G., Abraham, R., Merritt, A., et al. (2015). Forty-seven Milky Way-sized, Extremely Diffuse Galaxies in the Coma Cluster. ApJ, 798, L45.

van Gorkom, J. H. (2004). Interaction of Galaxies with the Intracluster Medium. In J. S. Mulchaey, A. Dressler, & A. Oemler (Eds.) *Clusters of Galaxies: Probes of Cosmological Structure and Galaxy Evolution.* p. 305.

Wendland, H. (1995). Piecewise polynomial, positive definite and compactly supported radial functions of minimal degree. Advances in Computational Mathematics, 4, 389–396.

Wetzstein, M., Naab, T., & Burkert, A. (2007). Do dwarf galaxies form in tidal tails? MNRAS, 375, 805–820.

Acknowledgments

It is no overstatement to say that the past year was a definitive period for my character. Working on my Master project gave me the necessary degree of self-confidence and helped me to find emotional balance. This positive development is attributed to a variety of people I have worked with and – fortunately enough – can continue to collaborate with in my upcoming PhD.

I am indebted to my supervisors Rhea-Silvia Remus and Klaus Dolag. Rhea, you gave me a fantastic science project, which inspired me to work on plots until deep in the night. Your guidance constituted an integral part for my progress and your honesty has saved me multiple times from descending into a downward spiral of self-doubts. Klaus, if it were not for your counsel, I could not have initialized even one simulation. You enabled me to enter the realm of computational astrophysics by providing kind and untiring patience for explanations, as well as physical intuition throughout my whole project.

I am thankful to Lucas Valenzuela for supporting me during my thesis. Your sixth sense for physics, as well as your programming advice in `Julia`[1] has contributed significantly to the level of my work. Together with the other members of the DRAGONS group – Silvio Fortuné, Benjamin Seidel and Lucas Kimmig – it is a joy to work with you! My sincere gratitude is also due to Tadziu Hoffmann for his readiness to help at literally a moment's notice – your insight both in astrophysics and numerics will never cease to amaze me.

I would like to thank Ludwig Böss for his repeatedly provided advice in numerical implementations, as well as Frederick Groth for his assistance in all kinds of programming questions. In that context, I warmly thank all CAST members for welcoming me in their group, taking me alongside them to most amusing conversations in the coffee breaks.

Finally, I want to express my utmost appreciation for my close friends and family. Your compassion and optimism has inspired me throughout the years and made life so much more entertaining. My dear parents: every of my achievements can be eventually traced back to your unconditional love and support. Thank you for accepting me the way I am.

---

[1] www.julialang.org

Selbstständigkeitserklärung

Hiermit erkläre ich, die vorliegende Arbeit selbstständig verfasst zu haben und keine anderen als die in der Arbeit angegebenen Quellen und Hilfsmittel benutzt zu haben.

München, 22. November 2023

_____

Anna Ivleva